Development of structured catalyst and reactor technologies for biomass conversion – Continuous production of sugar alcohols

Ali Najarnezhadmashhadi

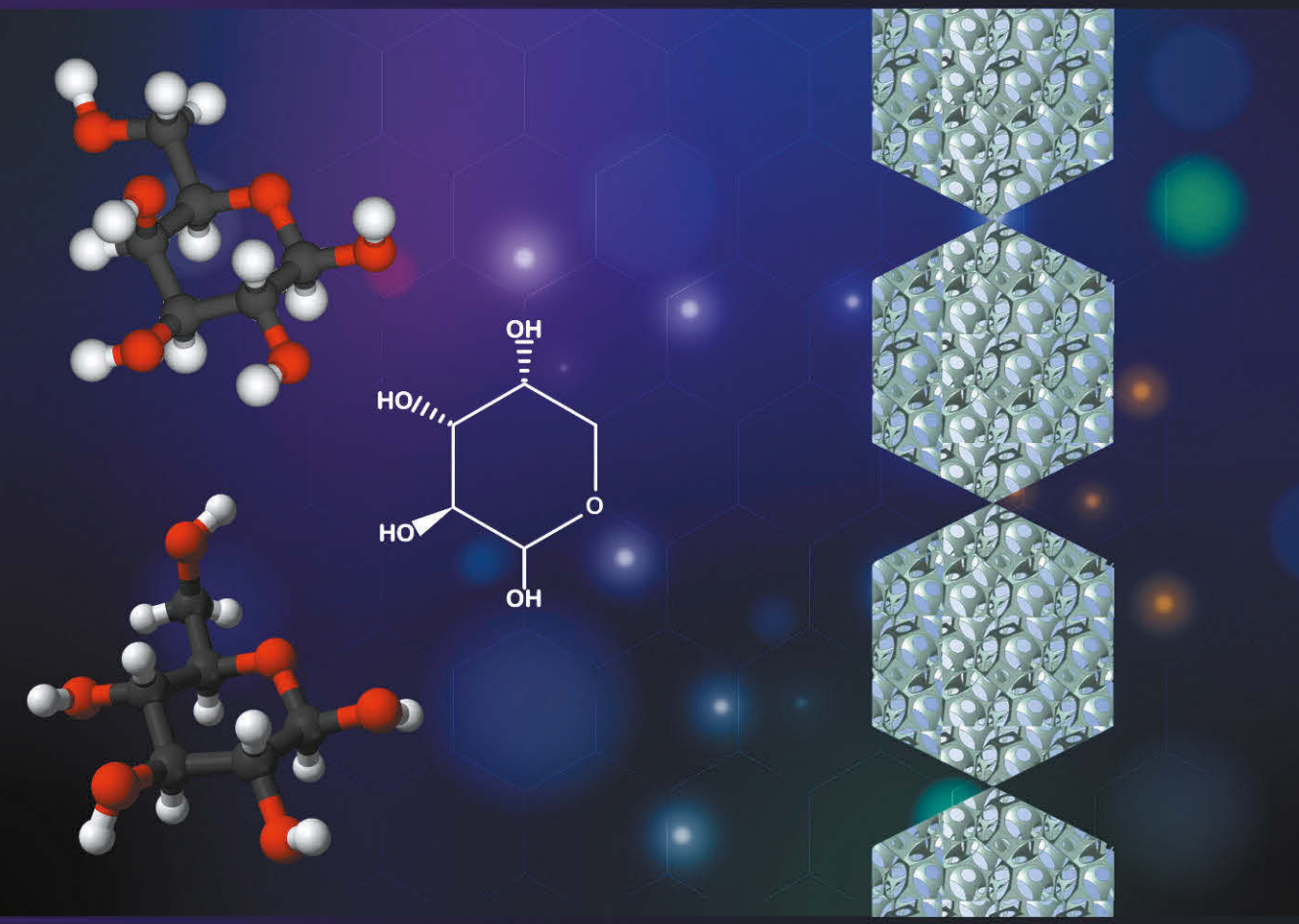

Laboratory of Industrial Chemistry and Reaction Engineering
Faculty of Science and Engineering/Chemical Engineering
Åbo Akademi University
2021

Ali Najarnezhadmashhadi

Born 1986, Mashhad, Iran

M.Sc. Chemical Engineering 2015
Åbo Akademi University, Turku/ Åbo, Finland

Development of structured catalyst and reactor technologies for biomass conversion - Continuous production of sugar alcohols

Ali Najarnezhadmashhadi

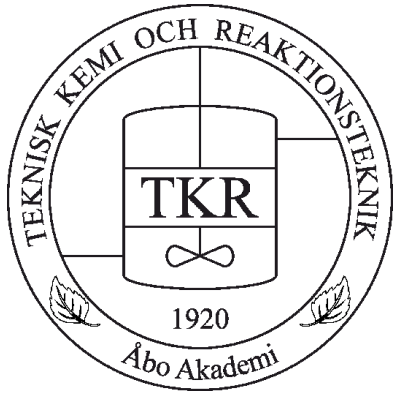

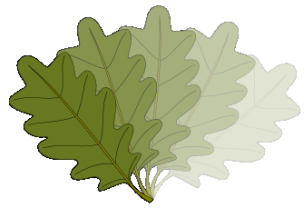

Johan Gadolin
Process Chemistry Centre

Laboratory of Industrial Chemistry and Reaction Engineering
Faculty of Science and Engineering/Chemical Engineering
Åbo Akademi University
Turku/Åbo, Finland, 2021

Supervised by

Academy Professor Dr. Tapio Salmi
Professor Dr. Dmitry Yu. Murzin

Laboratory of Industrial Chemistry and Reaction Engineering
Faculty of Science and Engineering/Chemical Engineering
Åbo Akademi University

Reviewers

Professor Dr. Juan Garcia Serna
Universidad de Valladolid
Valladolid, Spain

Docent Dr. Fredrik Sandelin
TF Engineers, Eura, Finland

Opponent

Professor Dr. Juan Garcia Serna
Universidad de Valladolid
Valladolid, Spain

ISBN 978-952-12-4049-2 (printed version)/ ISBN 978-952-12-4050-8 (electronic version)
ISSN 2669-8315 2670-0638

Acta technologiae chemicae Aboensia 2021 A/2

Painosalama Oy Turku/Åbo 2021

To the loving memory of my father

To my loving mother, and my lovely wife

“It is not the mountain we are conquering. It is ourselves”

-Sir Edmond Hillary

Preface

The completion of this thesis would not have been possible without the guidance and support of many people.

My first and foremost gratitude goes to Professor Tapio Salmi: Thank you so much for your constant support over all these years. I really appreciate your steadfast commitment towards research that could truly make a difference in the world. I admire your humble persona, scientific integrity, and your strong vision for your lab. You are also a great mentor. Under your supervision not only I learned to carry out research independently, but also to perform collaborative research in an effective manner. Besides fostering my independence and professional growth, your perennial positivity and encouragement for collaboration have made working in your group a joy. Whenever I have run into a road block along the way, you always seem to have that one key insight, question, or contact to get the wheels turning again. How can I ever thank you enough for all you have done for me? I am forever grateful. My special thanks go to Professor Dmitry Yu. Murzin: Thank you so much for your help, useful advice and insightful discussions during this work. You have provided support, guidance, and mentorship throughout my studies, always keeping your door open for me to discuss ideas and concepts. Our discussions have been an important factor in shaping and guiding my work.

Of course, my time in the laboratory could not have gone as smoothly as it did without the support of our Lab manager, Docent Kari Eränen. Thank you so much for your helpful assistance and support during my PhD. I would like to thank Professor Johan Wärnå for his great contributions in the kinetic modelling and simulations. I am also grateful to Dr. Atte Aho for his contribution in the catalyst characterization.

My one-year visit to the Chemical and Biological Engineering Department at the University of British Columbia in Vancouver gave a significant boost to the development of my research. I would like to offer a special thanks to the Professor Heather Trajano for the opportunity she gave me to work in her group. I am so grateful for her hospitality, support, and advice on my research.

Collaborative work with the other departments and institutes as well technical assistance from their personnel was an important element towards the successful completion of the present work. In this regard, I would like to thank Professor Henrique A. Matos and Dr. Catarina G. Braz from Universidade de Lisboa for accepting the idea of a collaborative work on modelling and simulation using gPROMS software. I am also grateful to Professor Vincenzo Russo from Università di Napoli 'Federico II' for his useful inputs and contribution in the simulations.

My sincere gratitude is rendered to all members of our laboratory, past and present, for providing a friendly and enjoyable working atmosphere. I am especially thankful to Pasi, Andrea, Erfan, Soudabeh, Adriana, Cezar, Nemanja, Ikenna and Ricardo for being friendly and supportive colleagues. I am also thankful to the colleagues in other research groups at Johan Gadolin Process Chemistry Centre.

Last but not least, to all my family members goes my deepest gratitude without whose unwavering support and continuous encouragement I would never have made it this far. Here, I am especially grateful to my mother, my father and my wife for their unconditional love and support during my study at Åbo Akademi. I greatly cherish the enthusiasm and encouragement they have shown, and continue to show, for every decision I have made in my life.

Abstract

Energy-efficient technologies have been an aspiration for chemical industries, especially the design of chemical reactors. Structured catalysts play an important role to achieve this purpose. Several types of structured catalysts have been invented and investigated in recent years, such as monoliths, fibers, solid foams as well as structures prepared by three-dimensional (3D) printing. Due to the fact that solid foam catalysts provide a high porosity (75-95%) and a high specific surface area, open cell foam catalyst packings have been investigated as an alternative for catalytically active reactor packings. Enhanced mass and heat transfer, suppressed pressure drop and high specific surface area are important positive features of the solid foam packings. Furthermore, the structures of pores and struts in open cell foams allow radial liquid flow and local vigorous turbulence which result in enhanced mass and heat transfer.

Development of a structured catalyst was performed successfully and ruthenium catalysts supported on carbon-coated aluminum foams (Ru/C) were prepared. First an active carbon support was prepared on open-cell aluminum foams. To incorporate a carbon layer into the aluminum foams, polymerization of furfuryl alcohol was carried out. The incorporation of ruthenium nanoparticles on the carbon coated aluminum foams was implemented by homogeneous deposition precipitation. Seven different characterization techniques such as SEM, TEM, XPS, TPR, ICP-MS, carbon monoxide chemisorption and nitrogen physisorption were applied on the solid catalysts.

The Ru/C foam catalysts were used in a continuously operating multiphase reactor set-up which had six tubular reactors working in parallel. Continuous hydrogenation of D-glucose, L-arabinose and a binary mixture of L-arabinose and D-galactose were studied in the experimental setup. Through investigating different reaction parameters, the temperatures 100-110°C and the liquid flow rates 0.5-1 mL/min were found suitable for catalyst screening and activity testing. The experiments were carried out at 20 bar hydrogen pressure. The continuous hydrogenation experiments were successful, the reproducibility was good, and the foam catalysts were stable. High selectivities of the desired products, sugar alcohols and sugar alcohol mixtures were obtained.

A mathematical model for open foam catalyst structures was developed. It was based on the concept of axial dispersion as the prevailing flow pattern, on liquid-solid mass transfer effects and intrinsic kinetics on the active sites of the catalyst. Rate equations were presented for the hydrogenation of individual sugars and binary sugar mixtures on Ru/C catalysts and they were implemented in the mass transfer and flow models of the open foam catalyst. The flow pattern in the foam structure was confirmed with step change experiments with an inert tracer.

A kinetic model for sugar hydrogenation was fitted to the experimental data obtained from open foam ruthenium catalysts. The non-competitive adsorption model was used for the adsorption of sugars and hydrogen. The effect of external mass transfer was included in the

model, because it is in practice impossible to completely eliminate the external mass transfer limitations in continuous operation of the shallow foam bed: in order to obtain a high enough liquid residence time, low liquid velocities were used.

Finally, a new advanced comprehensive and transient multiphase model for a trickle bed reactor with solid foam packings was developed where axial, radial and catalyst layer effects were combined. The unique feature of this model is that the gas, liquid and solid phase mass balances include most of the individual terms such as internal diffusion, gas-liquid and liquid solid mass transfer and intrinsic kinetics.

A very powerful software (gPROMS ModelBuilder) was used for the model development and implementation which provided rapid computations and parameter estimation results at a reasonable time. Parameter estimations for both models, including the activation energies and adsorption parameters were carried out. In all the cases, the confidence intervals of the parameters remained within 10% error, indicating a good accuracy of the parameters. To investigate the model performance, a sensitivity analysis was carried out and the effect of the kinetic parameters and the operation conditions on the arabinose and galactose conversions was studied in detail. The mathematical models developed and implemented in the present work are applicable for other three-phase research in continuous catalytic reactors with solid foam packings.

Referat

Utveckling av strukturerad katalysator- och reaktorteknologi för omvandling av biomassa – kontinuerlig produktion av sockeralkoholer

Ali Najarnezhadmashhadi

Energisnåla teknologier har blivit en önskan och ett mål för kemisk industri, speciellt projektering av kemiska reaktorer. Strukturerade katalysatorer spelar en aktiv roll då det gäller att nå detta mål. Olika typer av strukturerade katalysatorer har uppfunnits och undersökts under de senaste åren, t.ex. monoliter, fibrer, fasta skum och strukturer som har preparerats med hjälp av tredimensionell (3D) printning. Pga att fasta skumkatalysatorer har en hög porositet (75-95%) och specifik yta har skumkatalysatorer med öppna cellstrukturer undersökts som ett alternativ för konventionella katalytiska partiklar i packade bäddar. Effektiverad mass- och värmeöverföring, nedsatt tryckförlust och hög ytarea är viktiga positiva egenskaper för fasta skum. Dessutom möjliggör porstrukturen och väggelement ett radiellt vätskeflöde och intensiv lokal turbulens vilket resulterar i påskyndad mass- och värmeöverföring.

Utveckling av en strukturerad katalysator genomfördes framgångsrikt och rutenium-katalysatorer på kolbelagda aluminiumskum (Ru/C) preparerades i laboratorieskla. Först lades ett skikt av aktivt kol på öppna aluminiumskum. För att belägga aluminiumskummet med ett kolskikt polymeriserades furfurylalkohol på skummets yta. Ruteniumnanopartiklar fästes på kolbelagda aluminiumskum med hjälp av homogen avfällningsteknik. Sju olika metoder användes för att karakterisera de fasta katalysatorerna: svepelektronmikroskopi (SEM), transmissionselektronmikroskopi (TEM), fotoelektronspektroskopi (XPS), temperatur-programmerad reduktion (TPR), plasmamasspektroskopi (ICP-MS), kemisorption av kol-monoxid samt fysisorption av kväve.

De preparerade Ru/C-skumkatalysatorerna användes i ett kontinuerligt flerfasreaktorsystem som bestod av sex parallella tubreaktorer. Kontinuerlig hydrering av D-glukos, L-arabinos samt en blandning av en binär blandning av L-arabinos och D-galaktos studerades i den experimentella anläggningen. Efter att ha kartlagt olika reaktionsparametrar konstaterades temperaturerna 100-110°C och vätskevolymströmmarna 0.5-1 mL/min vara lämpliga för en närmare kartläggning av katalysatorer och undersökning av deras aktivitet och selektivitet. Kontinuerliga hydreringsexperiment var framgångsrika och reproducerbarheten var god och skumkatalysatorerna visade sig vara stabila. En hög selektivitet av de önskade produkterna, sockeralkoholer och blandningar av sockeralkoholer erhölls i experimenten.

En matematisk modell för öppna skumkatalysatorstrukturer utvecklades. Modellen baserar sig på axiell dispersion för beskrivning av strömningsbetingelserna, på vätske-fastfas massöverföringseffekter samt på reell kinetik på de aktiva säten på katalysatorytan. Hastighetsekvationer presenterades för enskilda sockerarter och sockerblandningar på Ru/C-katalysatorer och de implementerades i massöverförings- och strömningsmodeller för den öppna skumkatalysatorn. Strömningsbilden i skumstrukturen bekräftades med stegsvars-experiment med ett inert spårämne.

En kinetisk modell anpassades till data som erhållits från experiment med öppna skumkatalysatorer där rutenium var den katalytiskt aktiva metallen. En matematisk modell baserad på antagandet av icke-konkurrerande adsorption av sockerarter och väte användes. Effekten av extern massöverföring till katalysatorytan ingick i modellen, eftersom det är i praktiken omöjligt att fullständigt eliminera externa massöverföringsmotstånd i kontinuerlig drift av en kort skumbädd: för att uppnå tillräckligt höga uppehållstider av reaktionsvätskan är det nödvändigt att arbeta med låga vätskehastigheter.

En ny avancerad tidsberoende flerfasmodell för en tricklebäddreaktor packad med fasta skum utvecklades. Axiella och radiella effekter samt fenomen kopplade till katalysatorskiktet kombinerades i modellen. Den unika egenskapen av modellen är att ämnesmängdbalanserna för gas, vätska och fastfas innefattar de flesta individuella bidrag till systemet, såsom intern diffusion, gas-vätske- och vätske-fastfasmassöverföring samt reaktionskinetik.

En kraftig mjukvara (gPROMS ModelBuilder) användes för modellutveckling och implementering vilket möjliggjorde snabba datorberäkningar som gav parameterestimerings-resultat inom rimliga tider. Estimering av kinetiska parametrar, inklusive aktiveringsenergier och adsorptionsparametrar genomfördes med framgång. I alla estimeringar var parameterfelen inom 10%, vilket indikerade en god noggrannhet av parametrarna. För att undersöka modellens prestationsförmåga, utfördes en känslighetsanalys och effekten av kinetiska parametrar och driftsbetingelser i omsättning av arabinos och galaktos till motsvarande sockeralkoholer studerades i detalj. De matematiska modeller som utvecklades och implementerades i detta arbete kan i framtiden tillämpas på liknande forskning av trefassystem där fasta skum används.

List of of Publications

I. A. Najarnezhadmashhadi, K. Eränen, S. Engblom, A. Aho, D. Murzin, T. Salmi, Continuous Hydrogenation of Monomeric Sugars and Binary Sugar Mixtures on a Ruthenium Catalyst Supported by Carbon-Coated Open-Cell Aluminum Foam, *Industrial & Engineering Chemistry Research*, 59 (2020) 13450–13459.

II. A. Najarnezhadmashhadi, J. Wärnå, K. Eränen, H.L. Trajano, D. Murzin, T. Salmi, Modelling of kinetics, mass transfer and flow pattern on open foam structures in tubular reactors: Hydrogenation of arabinose and galactose on ruthenium catalyst, *Chemical* Engineering Science, 233 (2021) 116385.

III. A. Najarnezhadmashhadi, C.G. Braz, V. Russo, K. Eränen, A.H. Matos, T. Salmi, Modeling of three-phase continuously operating open-cell foam catalyst packings: sugar hydrogenation to sugar alcohols, Chemical Engineering Journal, (2021) (submitted)

Ali Najarnezhadmashhadi's (AN) contribution to articles I-III

I: AN made the experiments, interpreted the experiments and wrote and edited the article. II & III: AN gave the idea of the publication, contributed to the modelling, wrote and edited the manuscript

Conference publications related to the topic

I. A. Najarnezhadmashhadi, C.G. Braz, V. Russo, K. Eränen, H.A. Matos, T. Salmi, Dynamic modeling of an isothermal trickle bed reactor with solid foam packing: Sugar hydrogenation as a case study, *European Congress of Chemical Engineering*, ECCE13-ECAB6, 2021, Berlin – Germany – *Oral presentation*

II. A. Najarnezhadmashhadi, K. Eränen, J. Wärnå, T. Salmi, Continuous hydrogenation of sugar monomers and sugar mixtures with ruthenium catalyst supported on carbon-coated open-cell aluminum foam, *Catalysis in Multiphase Reactors – International Symposium on multifunctional Reactors*, CAMURE 11-ISMR10, 2021, Milano, Italy – *Oral presentation*

III. A. Najarnezhadmashhadi, C.G. Braz, V. Russo, K. Eränen, H.A. Matos, T. Salmi, Advanced modelling of a trickle bed reactor with solid foam packing: Arabinose hydrogenation as a case study. Advanced Process Modelling Forum (APM), 2021, Virtual event – *Poster presentation*

IV. A. Najarnezhadmashhadi, K. Eränen, T. Salmi, Development of new solid-foam catalysts for biomass conversion, Ali Najarnezhadmashhadi, Kari Eränen, Tapio Salmi, *27th Organic Reactions and Catalysis* ORCS27, 2018, San Diego,USA – *Oral presentation*

V. A. Najarnezhadmashhadi, K. Eränen, S. Engblom, A. Aho, D. Murzin, T. Salmi, Development of structured catalyst and reactor technologies for biomass conversion. 67th Canadian Chemical Engineering Conference, 2017, Edmonton, Canada – *Oral presentation*

VI. A. Najarnezhadmashhadi, K. Eränen, S. Engblom, A. Aho, D. Murzin, T. Salmi, New structured catalyst and reactor technologies for biomass conversion. Finnish Young Scientist Forum for Catalysis, 2016, Tampere, Finland – *Oral presentation*

Table of contents

1. Introduction

1.1. Background and state of art

The research in biomass valorization has become important because of shifting from fossil-based industry to the use of renewable raw materials. Biomass is known as a very good source of ecologically sound components [1, 2].

Hemicelluloses appearing in biomass are rich sources of basic sugars. Three main components of lignocellulosic biomass are hemicelluloses, lignin and cellulose. A lot of research is carried out in global scale on the transformation of cellulose to chemicals and fuel components, whereas hemicelluloses have to some extent been left in shadow. However, Nordic wood material contains up to 20% hemicelluloses, such as xylans, galactans and mannans (Figure 1). Recent research has shown that hemicelluloses can be efficiently and selectively separated from wood chips and wood powder by hot-water extraction. The mixture of hemicelluloses can then be hydrolyzed to sugar oligomers and monomers by using homogeneous, enzymatic or heterogeneous catalysts. The key issue here is to keep the hydrolysis conditions mild (less than 110ºC), so that low-molecular degradation products are avoided. It has recently been shown that this is possible. Typical hemicelluloses along with hydrolysis and hydrogenation products are listed in Table 1.

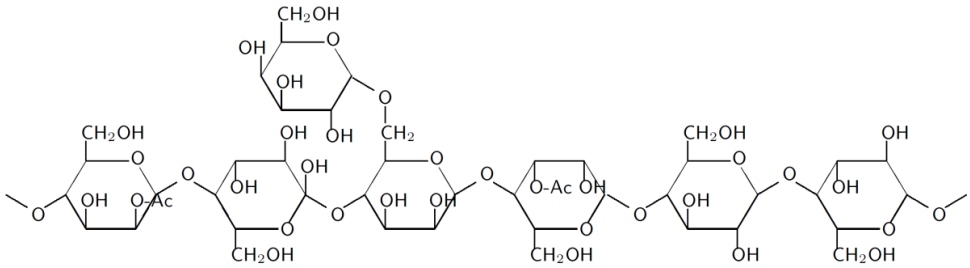

Figure 1. A typical hemicellulose: O-acetylgalactoglucomannan (GGM).

Table 1. Typical hemicelluloses, their hydrolysis and hydrogenation products

Arabinogalactan	arabinose, galactose	arabitol, galactitol
Arabinoglucuronoxylan	arabinose, xylose	arabitol, xylitol
Galactoglucomannan	galactose, glucose, mannose	galactitol, sorbitol, mannitol

A further treatment of the mixture of oligomers and monomers is really an issue. The components of the mixture can be separated, for instance, by preparative chromatography, by using simulating moving bed technology. However, for purposes, where a family of molecules of rather similar structures is desired, the hydrolysis mixture should be directly exposed to a catalytic treatment to obtain the target molecules. An evident example is hydrogenation of the monomeric and dimeric sugars to valuable sugar alcohols, which can be used for sources for valuable chemicals and fuel additives as well as sources for green hydrogen through aqueous-phase reforming [3].

Lignocellulosic biomass originating from wood, straw or bagasse is an abundant non-food source for chemical and petrochemical industry, but the conversion processes of lignocellulose to chemicals are often up-to-date ineffective and unprofitable. Processes based on the use of solid heterogeneous catalysts can provide the most selective routes for biomass conversion to high-value products. An ecologically friendly path for producing alternative sweeteners and health-promoting compounds is to apply catalytic hydrogenation of sugars to obtain the corresponding sugar alcohols [4]. Many of these processes are performed in aqueous solvents, where water-tolerable, highly active and selective catalysts are required. Molecules originating from biomass are quite large, which implies that diffusion resistance in the catalyst pores is considerably retarding the overall reaction rates. Current reactor technologies are not efficient enough for biomass conversion, as large catalyst pellets are used and they cause severe diffusion limitation.

New, more efficient catalyst structures are needed to improve the profitability of these processes. The new catalyst structures combine the benefits of the classical slurry and fixed bed technologies, having a thin and efficient catalyst layers and low pressure drop. Examples of these new structures are monoliths, solid foams and fibers [4]. Use of structured reactors is the key aspect in process intensification, leading to small, efficient and elegant equipment for chemical transformations. It is important to combine the catalyst and reactor technology with modern separation methods to reach sustainable technological, economical and ecological solutions.

1.2. Catalytic sugar hydrogenation

Controlled catalytic hydrolysis of starch, cellulose and hemicelluloses results in simpler carbohydrates (e.g. mono-and disaccharides), which can be valorized to components of practical importance by numerous processes, such as isomerization, hydrogenation and oxidation. Hydrogenation of sugars to sugar alcohols is a good example of such a process [5].

Sugar alcohols have many practical applications in the consumer society, for example as sweeteners, anti-caries and anti-inflammatory substances, additives in alimentary products and platform chemicals. Sugar alcohols can be prepared by reducing the carbonyl group in the sugar molecule. This can be done by the aid of chemical agents or using hydrogen molecules in the presence of heterogeneous and homogeneous catalysts [2].

Using the hydrogen molecule and a solid heterogeneous catalyst, no stoichiometric co-products are formed and cumbersome catalyst separation steps which are needed in case of homogeneous catalysts are avoided [2]. The application of heterogeneous catalysis and molecular hydrogen in the reduction of sugars follows the principle of green chemistry and green process technology. The reaction scheme is given below,

Sugar monomer + H_2 → *Sugar alcohol*

The reaction scheme is valid for the hydrogenation of various sugar monomers to the corresponding sugar alcohols, for example, for obtaining sorbitol from glucose, xylitol from xylose, arabitol from arabinose and galactitol from galactose. The hydrogenation reaction is in practise irreversible, but by-products, such as isomerisation products can appear, particularly in the lack for hydrogen in the reaction environment.

In the hydrogenation of sugars to sugar alcohols in industrial scale, the heterogeneously catalyzed process is preferred and catalysts based on Ni, Pd, Pt or Ru are mentioned in literature [2, 20, 9]. From chemical and physical viewpoints, ruthenium is a superior heterogeneous catalyst compared to sponge nickel in sugar hydrogenation, because ruthenium is active, selective and durable, whereas sponge nickel is poisonous, pyrophoric and subject to deactivation [6-19].

Heterogeneous catalysts, for instance, sponge nickel (Raney® Ni) activated with Pt, Pd, or Ru promoters are still used in the industrial sugar hydrogenation processes in both batch and continuous reactors [22]. Elevated pressures of hydrogen (30–50 bar) and temperature less than

150°C are needed in the process [8, 23]. A pitfall is that sponge nickel is pyrophoric and it suffers from severe catalyst deactivation due to leaching of promoters and accumulation of organic species on the active sites of the catalyst [12, 21]. The deactivation of sponge nickel, along with mathematical modelling is described in detail in ref. [7]. Nickel is toxic, hence it rises the purification costs when it leaches into the product solution, for instance in the sorbitol solution obtained in glucose hydrogenation. To overcome such problems, a different catalyst such as ruthenium supported on carbon can be used. [2, 24]. Other catalysts including Pt, Pd and Ru have been used for sugar hydrogenation, hemicelluloses and cellulose [22, 25]. However, in comparison with supported palladium, nickel or rhodium catalysts in glucose hydrogenation, supported ruthenium catalysts are the most active ones [12]. Furthermore, because of its good activity and excellent selectivity, ruthenium has been used as an active metal for sugar hydrogenation [2, 11, 26] and it is the most promising catalyst investigated so far [31]. Previous studies have also confirmed the significance of using Ru/C catalysts to convert non-lignocellulosic biomass derivatives to fuels [27-30].

1.3. Structured catalysts and reactors

Energy-efficient technologies have been an aspiration for the chemical industries, especially the design of chemical reactors. Structured catalysts play an important role to achieve this purpose. Several types of structured catalysts have been invented and investigated in recent years, such as monoliths, fibers, solid foams as well as structures prepared by three-dimensional (3D) printing. In a broad sense, many milli- and microreactors can be regarded as structured catalytic reactors. The characteristic feature for a structured chemical reactor is that the solid catalyst is kept immobile by fixing the catalyst carrier on the walls of the reactor channel (e.g. monolith and microreactor channels) or by installing the structured catalyst as an integrated part of the reactor tube.

For catalytic three-phase systems (solid catalyst, gas phase and liquid phase) the even distribution of the gas and liquid phases is a challenge for classical structured catalysts, such as monoliths. The distribution problem can be solved with tailored structures in laboratory scale, but the process scale up is demanding, because reliable and inexpensive distribution systems are required. Therefore, the interest in randomly organized structured catalysts, such as solid foams is growing. Simply speaking, if the solid catalyst itself is random, there is a hope that it helps to randomize the gas and liquid flows through the reactor. Solid foams have been

originally proposed for heat exchange, but in the recent years the interest in solid foam scaffolds for heterogeneous catalysts has been growing all over the world.

Hydrogenation of sugars in continuous devices has been previously reported, for example by Déchamp et al. [9], Eisenbeis et al. [10], Kilpiö et al. [11], Aho et al. [12], and Sifontes et al. [13], but they mainly used catalyst particles, monoliths, fibers, cloths and washcoated steel structures, but not open foams.

The hydrogenation process can be intensified using structured catalysts. Several types of structured catalysts have been developed over the last twenty years including monoliths, fibers, micro-structured catalysts and open foams [4, 30-44]. By using structured catalysts, the benefits of traditional slurry and packed bed technologies can be combined. Structured catalysts have very thin layers of the porous catalyst material, which suppresses the internal mass transfer resistance in the catalyst pores and gives high effectiveness factors and, structured catalysts have open structures which minimize the pressure drop [4]. With structured catalysts, both continuous and discontinuous technologies are enabled, whereas the slurry technology is in practice limited to batch and semibatch reactors. For catalytic hydrogenation of organic components, slurry and fixed bed technologies are used in large scale. The slurry technology utilizes very small catalyst particles (typically 10-50 micrometers), which efficiently suppresses the internal mass transfer resistance (pore diffusion). On the other hand, conventional fixed beds, where large catalyst particles (typically in mm and cm scale) are used have the benefit of a low pressure drop, but often they suffer from the serious disadvantage of internal diffusion resistance which impairs the catalyst effectiveness factor. Diminishing the particle size is a remedy, but it has a limit: with small particle sizes the pressure drop in the bed becomes too high and the operability is lost. Open foam catalysts represent avant-garde in catalysis and reactor technology with several benefits including simple preparation, randomization of gas and liquid flows in the open cell structure, high effectiveness factor, low degree of backmixing and low pressure drop [4, 30-44].

In the open catalyst structures, such as monoliths and solid foams the benefits of both classical slurry and fixed bed technologies are combined. Microreactors, monoliths, solid foams and fibers are examples of the new structures enabling very thin catalyst layers <<100 micrometer [4, 45]. The thin catalyst layer in a structured catalyst minimizes the resistance of internal diffusion in the catalyst pores. Quantitatively, the Thiele modulus is proportional to the catalyst layer thickness; by shifting to thinner and thinner layers, the Thiele modulus is diminished and

a catalyst effectiveness factor close to 1 can be achieved, which implies operation under kinetic control. The open architecture of structured catalysts guarantee a low pressure drop.

The large surface-to-volume ratios in metal foams make them suitable for catalytic applications [40]. The heat transfer efficiency is improved significantly by the high conductivity of metallic open-cell foams compared to the ceramic foams [40, 46]. Another advantage of metal foams is radial mixing inside their structure comparing with honeycomb monoliths [40]. Radial mixing improves the mass and heat transfer characteristics of the foams [35] and prevents the appearance of radial temperature gradients in the reactors. Most open-cells foams are made out of copper, aluminum, nickel or metal alloys. Ultra-light materials such as aluminum foams have a high porosity and a low bulk density. A schematic view of a foam structure is provided in Figure 2.

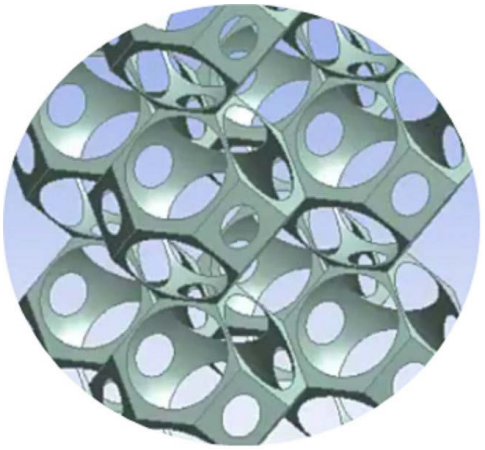

Figure 2. Geometry of Kelvin cell packing.

The high surface area-to-volume ratio in the metal foams increases the transfer of heat between the solid and the fluid. The low density, lightweight, high heat conductivity, low electrical conductivity, enhanced local flow mixing, high porosity and resistance to shock and deformation make metal foams very appropriate for various applications both in laboratory and industrial scale [33, 37, 47].

1.4. Research objectives

The objective of this PhD project was to develop new structured catalysts and reactors for the conversion of real sugar monomer and oligomer mixtures by heterogeneously catalyzed hydrogenation to valuable sugar alcohols. Moreover, advanced three-phase catalytic tubular reactor models were developed for solid foam packings. The models described in this work are applicable for other three-phase research in continuous catalytic reactors with solid foam packings.

Developing a structured catalyst was performed successfully and carbon-coated aluminum foams supported ruthenium catalysts were prepared, characterized and tested. Hydrogenation experiments of glucose, arabinose and binary mixtures of arabinose and galactose in a tubular reactor packed with open cell aluminum foam catalysts were successfully performed.

Molecular hydrogen was used as the environmentally friendly hydrogenation agent, which implies that no harmful stoichiometric co-products were formed. The reaction solvent was water. The concept applied in this work is inherently green: the reactants, the products and the process fulfill all the classical requirements for green chemistry and green process technology.

The following hypotheses were considered. The large surface to volume ratios in the metal foams make them suitable for catalytic applications. The heat transfer efficiency is improved significantly by the high heat conductivity of metallic open-cell foams compared to ceramic foams. Another advantage of metal foams is radial mixing inside their structures compared with honeycomb monoliths. Furthermore, the structures of pores and struts in open cell foams allow radial liquid flow and local turbulence which result in enhanced mass and heat transfer. In comparison with solid particle packings, solid foams have higher overall mass and heat transfer rates. Moreover, axial and radial mixing are improved by the high pore tortuosity of solid foams. Thin catalyst layers (typically << 10 micrometer) used in solid foams improve the internal mass transfer in the catalyst pores, which leads to higher effectiveness factors compared to catalyst pellets with thicker catalyst layers (up to 1 cm). Based on the characteristic features mentioned, open cell foam catalysts are valuable as reactor packing materials and beneficial for continuous tubular reactors.

2. Experimental section

2.1. Catalyst development

Carbon-coated aluminum foams supported ruthenium catalysts were prepared, characterized and tested.

To transform the open cell foam into a working catalyst support, it is necessary to deposit a high surface area washcoat on the foam so that a micro-mesoporous structure is created, on which a highly catalytically active species, such as metal nanoparticles can be deposited [48]. Pure aluminum foams were used for coating the aluminium foams with carbon. The pore density of the foams was 40 PPI (Goodfellow Cambridge Ltd.). The foams were cut into cylindrical pieces with a dimension of 33 mm length × 11 mm diameter using a diamond hole saw bit.

A controlled procedure for the furfuryl alcohol polymerization needed to be used to create a homogeneous layer of polymer on the foam and to prevent the open structure getting clogged. Furfuryl alcohol as a precursor and oxalic acid were used for carbon coating. 13.5 g distilled water, 110 g furfuryl alcohol (Sigma Aldrich; 98 %), and 0.34 g oxalic acid dihydrate (Sigma Aldrich; 99.5 %) were mixed in a 250-mL glass beaker. To clean the foam samples, they were kept in an ultrasonic bath filled with distilled water for 20 minutes and dried at 70 °C for 2 h. A hot plate stirrer was used to heat the mixture to the desired temperature. While the foams were rotated at 370 rpm constantly, the mixture was heated to 110 °C. The centrifugal forces prevented clogging of the polymer. Finally, for removing the excess polyfurfuryl alcohol (PFA), the foams were taken out from the PFA solution and centrifuged in another beaker. As the temperature of the foam sample had decreased to room temperature, the foams were pyrolyzed in a furnace (Carbolite CTF 12/100/900) for 5h at 550 °C in a nitrogen stream with a flow rate of 1 L/h. The activation was carried out under an air flow of 5 L/min at 380 °C for 2 h. Images of the aluminum foams before coating, after coating and after activation are presented in Figure 3.

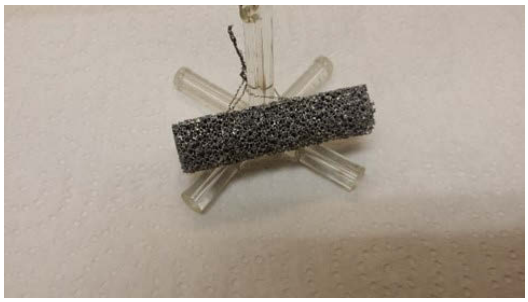

(a)

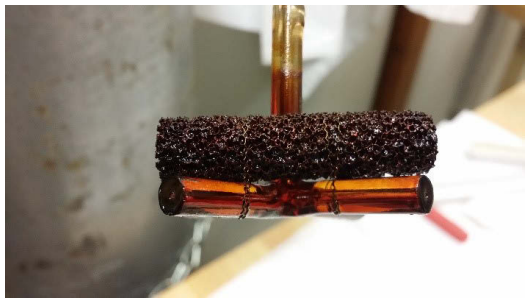

(b)

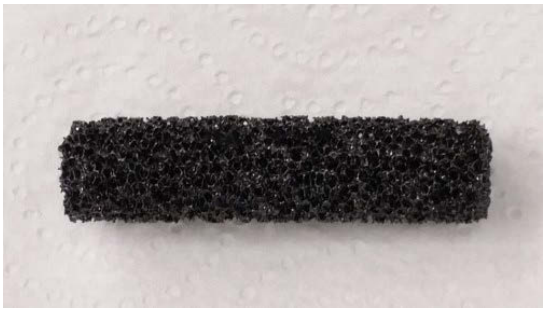

(c)

Figure 3. Samples of 40 PPI open-cell aluminum foam (a) before polymerization step, (b) after polymerization step and (c) after activation.

2.1.1. Deposition of ruthenium

To deposit ruthenium on the carbon-coated foam samples, the Homogeneous Deposition Precipitation (HDP) method was used. Through the HDP process, the pretreated carbon-coated foam was in a solution precursor (Ru 1.5 – 2 wt%) and urea in distilled water. The Ru/urea molar ratio was 1:5. A pH meter (Radiometer PHM 220) was used to monitor the pH of the process and a pH sensor was immersed in the solution during the entire process. The solution was heated to 80 °C while stirring constantly. The HDP process was continued for 24 h and the pH-values were frequently monitored and recorded during the process with a PC. Nitric acid (5 wt%) was used to pretreat the carbon coated foams. After completing the HDP process, the foams were activated in a tubular furnace at 450 °C under hydrogen atmosphere.

2.1.2. pH measurement in the HDP process

Change of the pH values of the solution for the three loaded 40-PPI foam were measured. After 24 hours, the solution with the foam samples reached a constant pH value. The foams were pretreated with different nitric acid concentrations (65, 34 and 5 wt%) to functionalize them by oxidation and enable the deposition of ruthenium. The treatment was carried out at 22 °C (room temperature) for 2 hours.

2.2. Catalyst characterization

Several physical and chemical techniques were applied to characterize the catalyst samples: Scanning Electron Microscopy (SEM), Transmission Electron Microscopy (TEM), X-ray Photoelectron Spectroscopy (XPS), Temperature Programmed Reduction (TPR), Inductively Coupled Plasma Mass Spectrometry (ICP-MS), CO chemisorption and nitrogen physisorption.

2.2.1. Nitrogen adsorption

The specific surface areas were determined by nitrogen adsorption (Sorptometer 1900, Carlo Erba instruments). The catalysts were outgassed at 150 °C for 3 h before the analysis was started. To calculate surface areas of microporous and mesoporous materials, BET and Dubinin equations were applied, respectively.

2.2.2. Scanning Electron Microscopy (SEM)

The SEM (Zeiss Leo Gemini 1530) images gave information on the surface structures of the aluminum foam, and the foam deposited with a carbon layer. Using Jeol JXA- 8530F field emission electron probe microanalyser, images with 5 kV acceleration voltage were taken.

2.2.3. Transmission Electron Microscopy (TEM)

Electron microphotographs of the catalysts were obtained with a JEM 1400 Plus, 120 kV acceleration voltage and resolution of 0.38 nm equipped with OSIS Quemesa 11 Mpix bottom mounted digital camera.

2.2.4. Measurement of ruthenium loading

ICP-MS (PerkinElmer SCIEX - ELAN DRC PLUS) was implemented to gauge the concentration of Ru deposited on the foams. Two liquid samples were withdrawn from the solution in order to measure the Ru concentration; one was a sample before starting the deposition and the other sample was withdrawn at the end of the HDP. Samples were dissolved in a microwave oven, acids (3 mL HNO_3 (65%) + 3 mL HCl (30%)) added and diluted to 100 mL before the ICP analysis. The assumption was that the difference in the two concentrations represents the amount which was completely deposited on the foam sample.

2.2.5. CO chemisorption

The metal cluster size was determined by CO chemisorption using a Micromeritics AutoChem 2910 device. A tubular furnace at 450 ºC with a hydrogen atmosphere was used to reduce the samples prior to the CO chemisorption. The CO chemisorption was first done by reducing the catalyst at 110 °C for 2 h where the heating rate was 10 °C/min. Pulses of CO were injected to the sample at 25 °C until the TCD peaks were of constant size.

2.2.6. X-ray Photoelectron Spectroscopy (XPS)

To reveal the oxidation state of Ru on the surface of the catalyst, XPS was used. XPS-analysis carried out by a Perkin-Elmer PHI 5400 spectrometer with a Mg K-alfa X-ray source operated at 14 kV and 200 W. The binding energy calibration was based on the Al 2p peak. Xpspeak4.1 program was used for the peak fitting.

2.2.7. Temperature Programmed Reduction (TPR)

The TPR experiments were conducted with 5 °C/min to 700 °C in which the reduction was started at approximately 200 °C. Based on the TPR experiment carried out in this study and also the procedure proposed by Thakur et al. [49], to use 500 °C, the foams were reduced in a tubular furnace under hydrogen atmosphere at 450 ºC.

2.2.8. Mechanical stability of the coated foams

The mechanical stabilities of the coated foams were measured in a stirred tank. The foam samples were attached to the cross-shaped stirrer shaft by a stainless-steel wire. To determine the mechanical stability of the coating material, foams were rotated for one hour at the speed of 500 rpm in distilled water. Before and after this experiment, the sample was dried and weighed and it had not changed, thus confirming the mechanical stability of the foam.

2.3. Parallel screening in multiphase reactor set-up

Hydrogenation of glucose, arabinose a mixture of galactose and arabinose were successfully carried out in a laboratory-scale screening equipment, with six continuously operate parallel reactors, in which the foam catalysts were placed. The reactor system is displayed in Figure 4. The reactor tubes had inner diameters of 12 mm and 120 mm lengths for the heated parts. To measure the temperature inside the reactor tubes a K-type thermocouple was used. The thermocouple tip was in contact with the lowest piece of the foam catalyst. To pump the sugar solution, individual pumps (flow rate of 10.0 ml/min was the maximum, Knauer Smartline 100) were used. The pressure of reactors was measured and monitored by a controller (Brooks Instrument 5866). The liquid eluents from the reactors were collected in 150 ml vessels. The experiments were conducted under isothermal conditions and under a constant hydrogen pressure at 20 bar. The flow rates of aqueous sugar solutions were 0.5–2 mL/min, the hydrogen flow rate was 25–100 mL/min and the temperature interval of the experiments was 90–120°C. The inlet sugar concentrations were varied between 0.13–0.66 mol/L. The isothermal reactor system was operated in a continuous mode and samples were withdrawn at the reactor outlet. Sampling was done by a sampling valve system through the experiments. Samples were withdrawn after 30, 60, 90, 120, 150 and 180 min. The concentrations of the reactants and products were analyzed with high performance liquid chromatography (HPLC, HP 1100 Series LC).

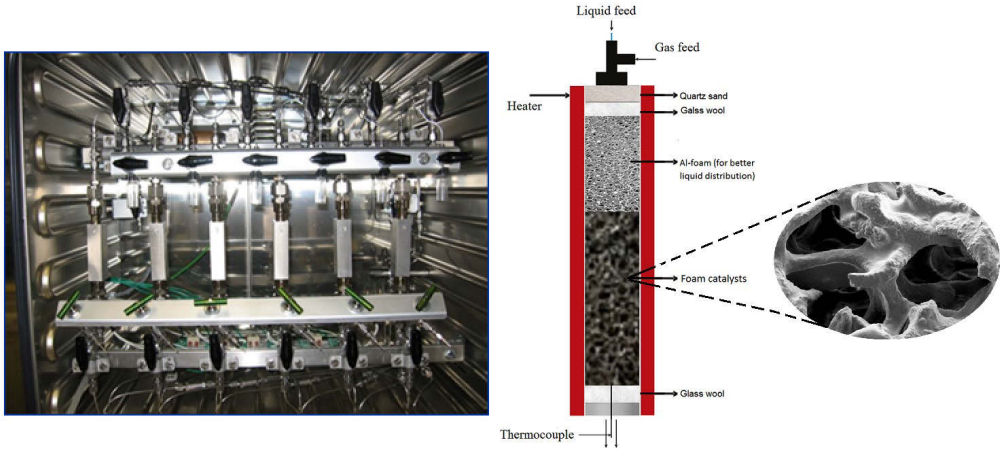

Figure 4. Reactor system consisting of six parallel tubes and filling of the reactor tube.

2.4. Residence time distribution measurements

The residence time distribution (RTD) measurements were carried out to determine the flow pattern. The structure of the reactor system was the same as in the hydrogenation experiments. To determine the RTD, step response experiments with two different liquid volumetric flow rates were carried out. A KCl standard solution as an inert tracer and de-ionized water were used to perform the experiments. The liquids were fed to the reactor system using a HPLC pump (Knauer Smartline 100) and hydrogen was fed using a mass flow controller (Brooks Delta Series). During the step response experiments, the concentration of the tracer was recorded at every two seconds by a conductivity meter (Radiometer CDM210, Radiometer Analytical)) at the outlet of the reactor.

The step response experiments were carried out in the following way: de-ionized water was pumped through the reactor at 0.5 and 1 ml/min together with a hydrogen flow at 25 ml/min at atmospheric pressure. After attaining a steady state, the pump tube was suddenly shifted from water to the KCl standard solution and at the same time the data logging of the conductivity was commenced.

2.5. Pressure drop

The continuously operated tubular reactor was packed with foams as illustrated in Figure 4, with one uncoated foam at the top and two coated foams at the bottom. The gas used was argon and the liquid was distilled water. The gas flow rate was controlled by a mass flow controller (Brooks 5850S) and the liquid was pumped to the reactor with an HPLC pump (Knauer Smartline 100). Downward concurrent gas and liquid flows were applied and the gas and liquid passed through the foams in the sequence: uncoated foam – first coated foam – second coated foam. A pressure sensor (Keller PR21S sensor with the range 0-2.5 bar (g) and output 4-20 mA) was located upstream of the reactor in the gas feed line. A CAL9500P controller (West Control solutions) was used to convert the 4-20 mA signal to a pressure value.

3. Results and discussion

3.1. Catalyst preparation, characterization and screening

Carbon-coated aluminum foams supported ruthenium catalysts were prepared, characterized and tested. Previous research describes various procedures to increase the size of the surface areas of the foams by producing porous titania and alumina washcoats and zeolite layers on the open cell foams [34, 50, 52]. The use of a carbon porous layer on open-cell foams as catalyst support has been previously investigated [36, 38, 39]. Vergunst et al. [32], proposed carbon coating of structured substrates. They coated honeycomb monoliths and used polyfurfuryl alcohol (PFA) as carbon precursor. The furfuryl alcohol is advantageous because it is made of renewable biomass [30]. Using a modified method from Toebes et al. and Lali et al. [30, 51], ruthenium was dispersed on highly porous structures in the current work.

3.1.1. Specific surface area and preparation conditions for the foam samples

The specific surface areas and carbon loadings for eight different groups of catalysts are reported in Table 2. The results illustrate that the exposure time between 110 °C and 120 °C had an effect on the carbon loading. This study focused on the foam samples with an average carbon loading of 10 wt% (sample types C, D and E).

Table 2. Carbon loadings and specific surface areas of selected catalysts.

Sample	m_{sample}[g]	Loading [wt%]	Time [min]		Specific surface area [$m^2 g_{coating}^{-1}$]
			20-110 °C	110-120 °C	
A	0.9163	10 %	55	35	135
B	0.8878	9 %	50	35	143.9
C	0.8915	10 %	55	40	140.9
D	0.8964	10 %	55	40	214.3
E	0.962	10 %	55	40	198.9
F	1.04	26 %	55	45	122
G	0.9098	25 %	55	55	90.98
H	1.0359	30 %	55	55	73

3.1.2. Carbon coated layer

Washcoat layer uniformity was studied by SEM. The SEM images showed in Figure 5 display the surface structures of the aluminum foam and the foam deposited with a carbon layer. The figure indicates that an even carbon layer had been formed on the aluminum surface and that the cell structure had remained open during the deposition process.

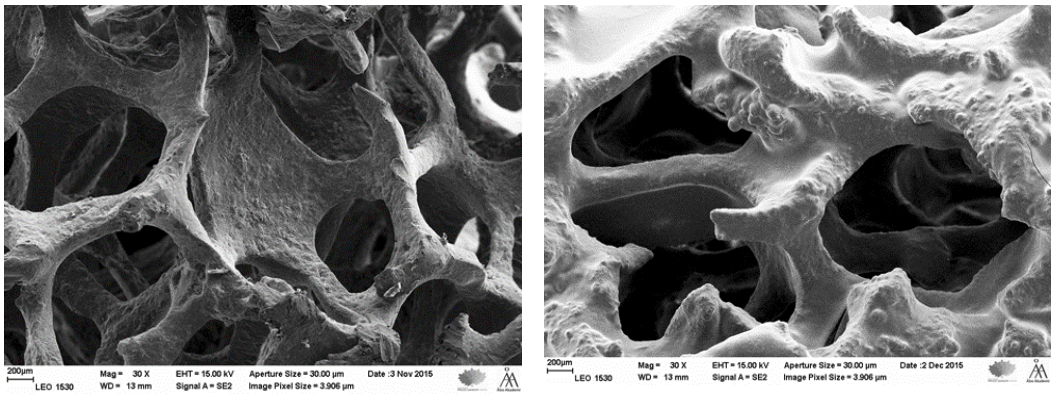

(a) *(b)*

Figure 5. Surface structure of a carbon coated foam substrate: (a) is SEM image of the surface structure before coating, (b) is SEM image after coating.

3.1.3. Catalyst particle size

The samples had to be crushed to powder in order to be investigated by high-resolution TEM. The coating layer of the foams were then scratched but also aluminum foam particles got scratched and mixed in the powder which made it difficult to recognize the real cluster size by TEM. Then, the cluster size was measured by CO chemisorption (AutoChem 2910). The active particle diameter was 2.34 nm. Some TEM images of the catalysts screened are shown in Figure 6.

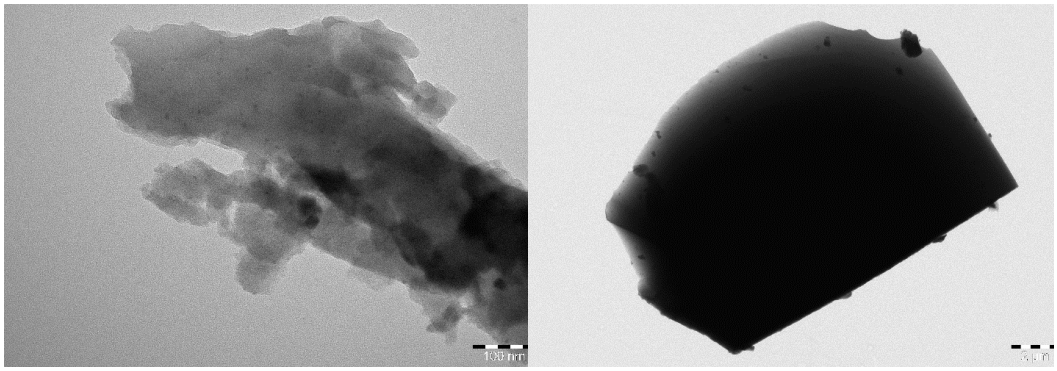

Figure 6. Transmission electron microscopy (TEM) of the ruthenium catalysts.

3.1.4. Foam pretreatment

The foams were pretreated with different nitric acid concentrations (65, 34 and 5 wt%) to functionalize them by oxidation and enable the deposition of ruthenium. The treatment was carried out at 22 °C (room temperature) for 2 hours. After 24 hours, the solution with the foam samples reached a constant pH value. The changes of the pH values of the solution for the three loaded 40-PPI foam samples are illustrated in Figure 7. The results remarkably revealed that the pH of the solution for samples 1 (treated with 65 wt%) and 2 (treated with 34 wt%) did not reach a constant level at pH 7 during 24 hours. However, there was a smooth change of pH for sample 3 (treated with 5 wt%) until a plateau was reached at pH 7. Therefore, to have a gradual change in pH through the deposition process, nitric acid concentration of 5 wt% was used to pretreat the foams.

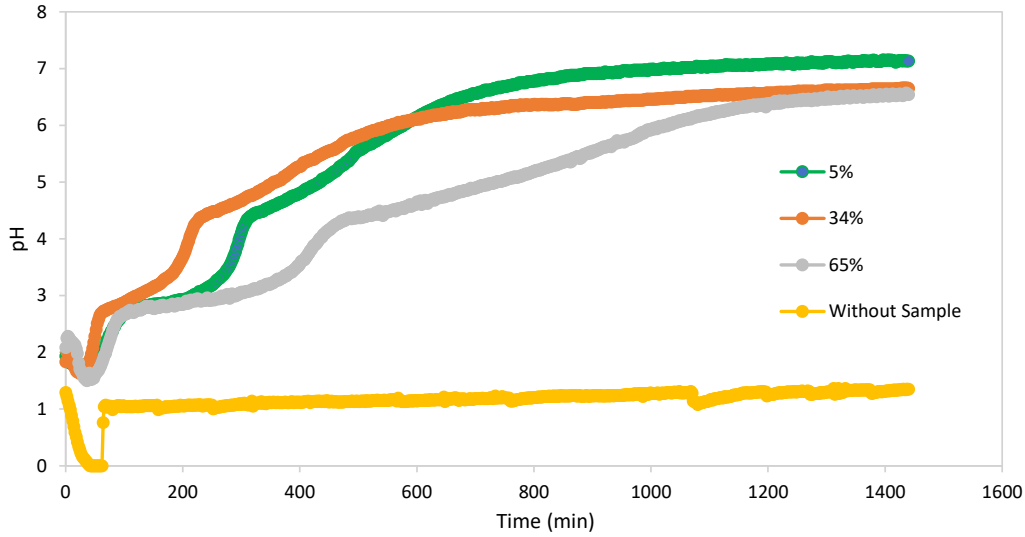

Figure 7. Variation of pH during 24 h of HDP.

3.1.5. Oxidation state of ruthenium

XPS spectra of the ruthenium catalysts are displayed in Figure 8. As revealed by the XPS spectra, ruthenium on the carbon surface after HDP is mostly exists as RuO_2 and $Ru(OH)_3$. To attain elemental ruthenium, the foam catalysts need to be reduced. Thus, the reduction temperature for the samples was investigated using TPR (AutoChem 2910) equipped with a thermal conductivity detector (TCD). The TPR experiments were conducted with 5 °C/min to

700 °C in which the reduction was started at approximately 200 °C. Based on the TPR experiment carried out in this study and also the procedure proposed by Thakur et al. [49], to use 500 °C, the foams were reduced in a tubular furnace under hydrogen atmosphere at 450 ºC.

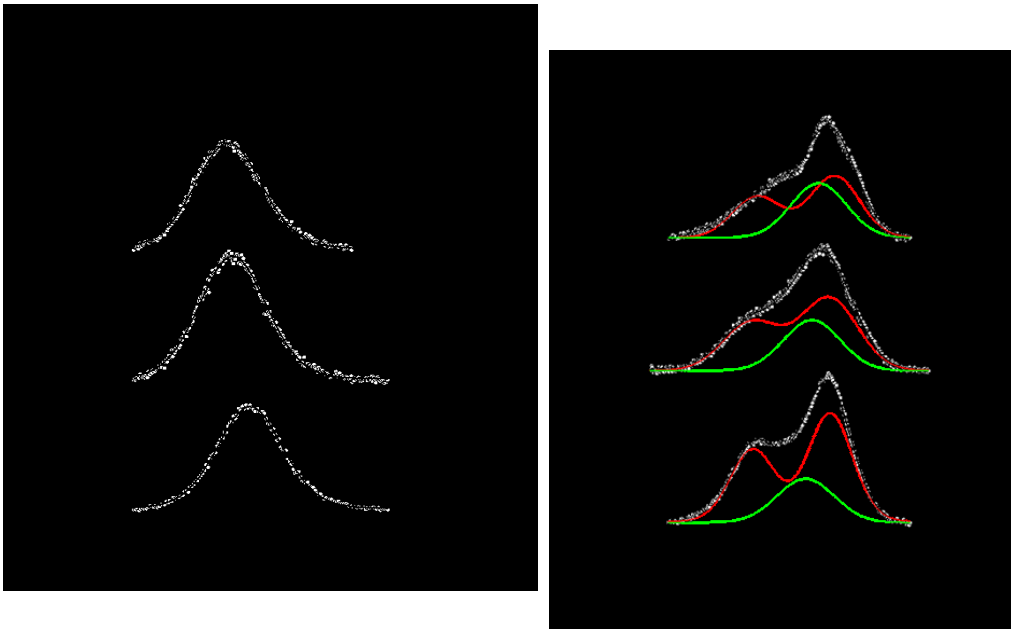

Figure 8. XPS spectra of the ruthenium catalysts.

3.2. Sugar hydrogenation in continuous mode

The main goal of this work is to demonstrate the feasibility of the open-foam catalyst in continuous and selective hydrogenation of sugar monomers and sugar mixtures to sugar alcohols. Sugar mixtures were studied because they are evident raw materials for the hydrogenation process: hydrolysis of a hemicellulose consisting of different sugar units gives always a mixture of various monomers, for example, hydrolysis of arabinogalactan leads typically to a 1:5 molar mixture of arabinose and galactose. Sugar alcohols have numerous industrial and consumer applications. To produce polyurethanes, polyesters and alkyd resins sugar alcohols can be used. Moreover, they are key intermediates in manufacturing pharmaceuticals and in synthesis of ligands [2, 53]. Sugar alcohols are very good sweeteners and have anti-inflammatory and anti-caries effects [1, 45]. The focus was in the preparation of sorbitol, arabitol and galacticol from sugar monomers and monomer mixtures.

3.2.1. Continuous hydrogenation of glucose

Hydrogenation of glucose to sorbitol was carried out on the carbon-coated aluminum foam supported ruthenium catalysts in the multiphase reactor set-up (Figure 4). To screen the reaction conditions, the temperature was varied between 90 to 120 °C while the hydrogen pressure was kept constant at 20 bar, because previous research has indicated a rather minor effect of hydrogen pressure on the hydrogenation rates of sugars [2]. All six reactors were used simultaneously, and each reactor had two foam catalysts (sample types C, D and E according to Table 2). All the foam catalysts were prepared under exactly identical conditions. Samples were taken every 30 min, a total of six samples for each reactor. Figure 9 shows the temperature dependence of the sorbitol productivity at different temperatures with the glucose concentration of 0.16 mol/L and 20 bar hydrogen. The selectivity to sorbitol at 90 ºC was 100% and 96% at 100 ºC. The experimental data in the figure are averages from multiple samples.

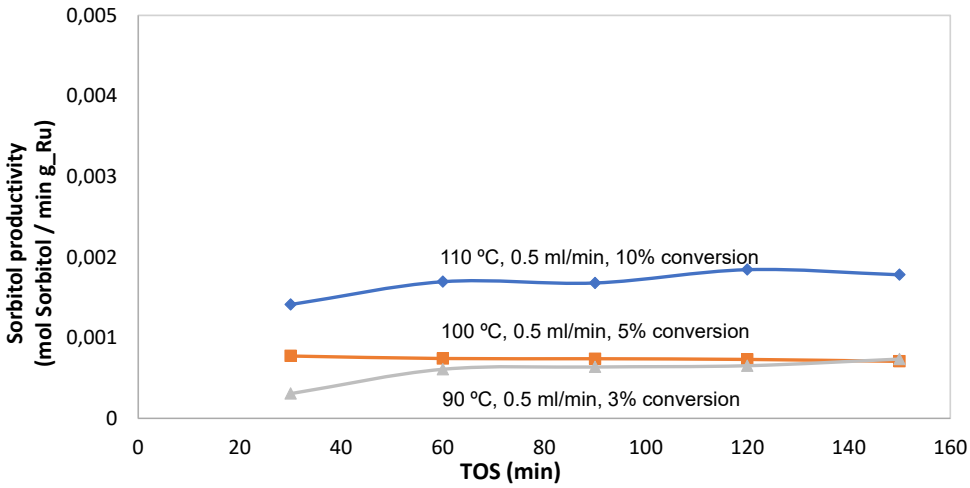

Figure 9. Sorbitol productivity at different temperatures.

The temperature effect was very expected which demonstrates the influence of the reaction temperature on the hydrogenation performance. This observation is in complete accordance with the previous experience [2] of sugar hydrogenation on ruthenium catalysts as slurries. Due to the short residence time in the tubular reactor, the conversion of glucose was 10% or less.

Using a Ru/C foam catalyst in a rotating foam reactor, Lali et al. [49], reported 2.5 % conversion of glucose at 100 ºC.

3.2.2. Continuous hydrogenation of L-arabinose

L-arabinose was hydrogenated to arabitol on the carbon-coated aluminum foam supported ruthenium catalyst in the continuously operated reactor system (Figure 4). The influence of the initial arabinose concentration (2-10 wt%, corresponding to 0.13-0.66 mol/L in water) on the arabitol productivity is illustrated in Figure 8. Additional hydrogenation experiments were conducted out by changing volumetric flow rates (0.5-2 mL/min). The experimentally recorded sugar conversions in the figures are averages from multiple samples.

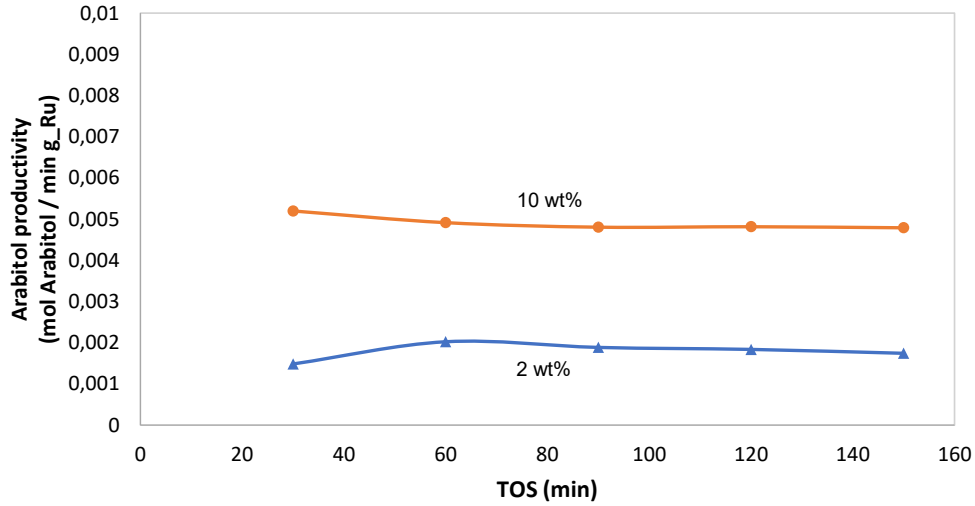

Figure 10. Arabitol productivity at different L-arabinose concentrations at 110 ºC and 20 bar hydrogen.

The conversion of L-arabinose with the initial concentration of 0.13 mol/L at 110 ºC was 13.7 % and the selectivity of arabitol at 90ºC was 99%, at 100 ºC it was 95% and at 110 ºC was 89%. The effect of the reaction temperature on the arabitol productivity is shown in Figure 11.

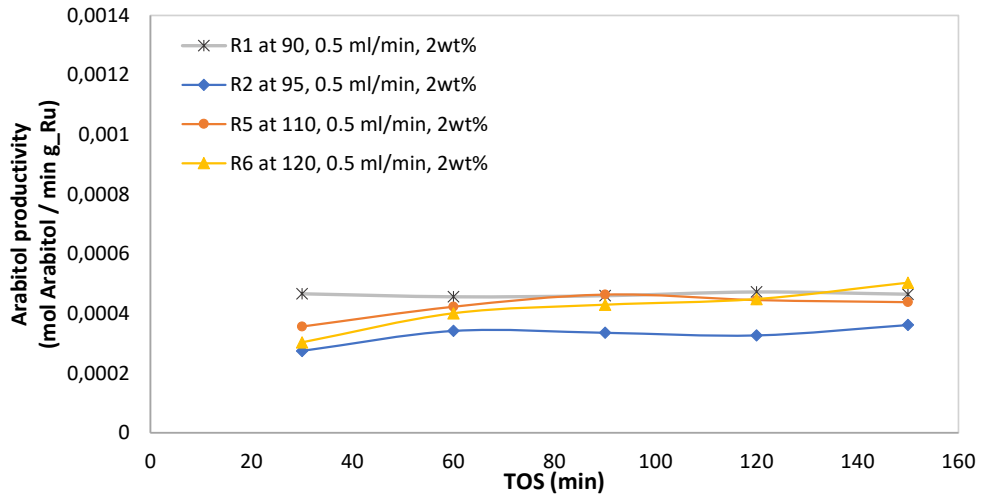

Figure 11. Temperature dependence of the arabitol productivity using 0.13 mol/L aqueous L-arabinose.

A higher arabitol productivity was observed when the hydrogenation was conducted at higher temperatures, which is in accordance with previous studies carried out with ruthenium catalysts in slurry reactors [2]. The experiments were repeated several times and the reproducibility was good. Figures 12 and 13 demonstrate the influence of the flow rate at 110-120 ° C on the arabitol productivity.

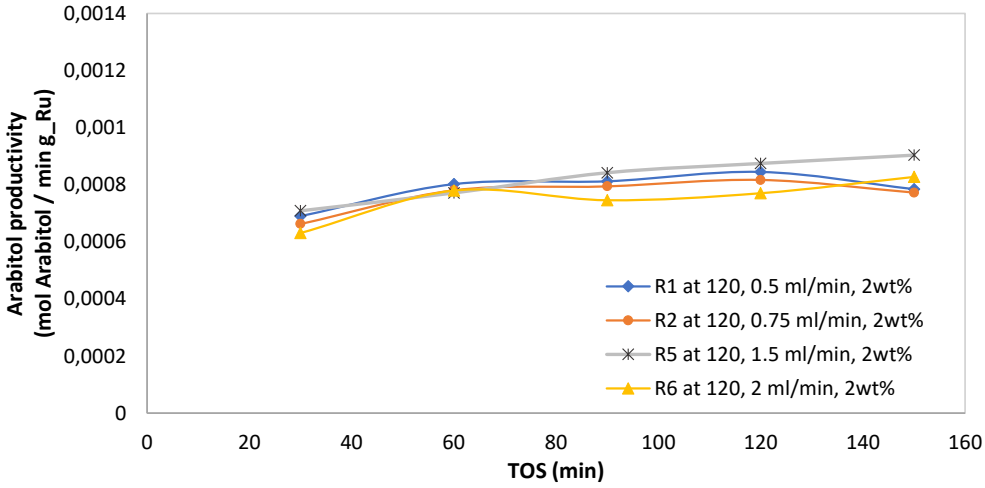

Figure 12. Arabitol productivity using 0.13 mol/L aqueous L-arabinose at different flow rates at 120 ºC.

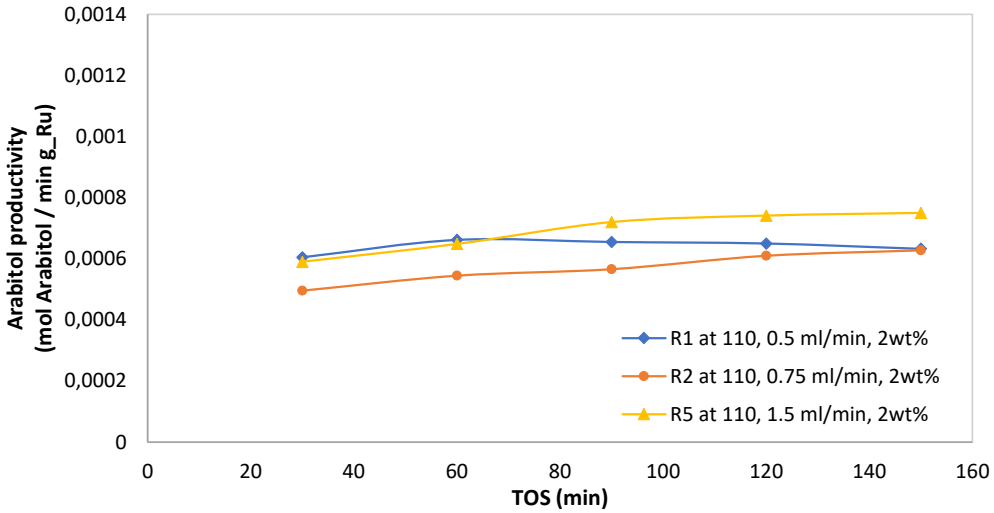

Figure 13. Arabitol productivity using 0.13 mol/L aqueous L-arabinose at different flow rate at 110 ºC.

The effect of flow rate was less pronounced, on the other hand, it was not possible to vary the flow rate in the current experimental domain in very large space.

3.2.3. Continuous hydrogenation of sugar mixtures

The mixture effect on the hydrogenation kinetics of L-arabinose and D-galactose mixtures was studied at different temperatures (90–120 °C), and molar ratios of D-galactose and L-arabinose (1, 2, and 5). The influence of the reaction temperature on the sugar conversions are shown in Figure 14. The experimentally recorded sugar conversions in the figures are averages from multiple samples.

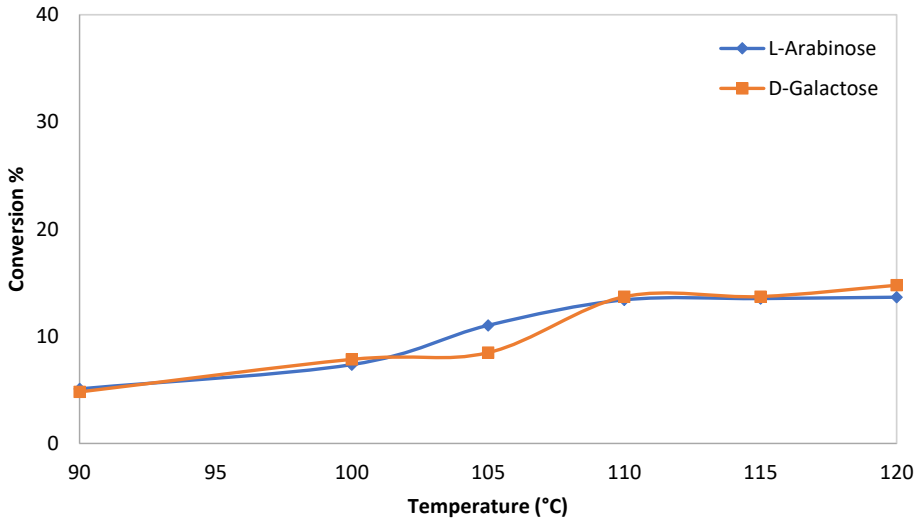

a)

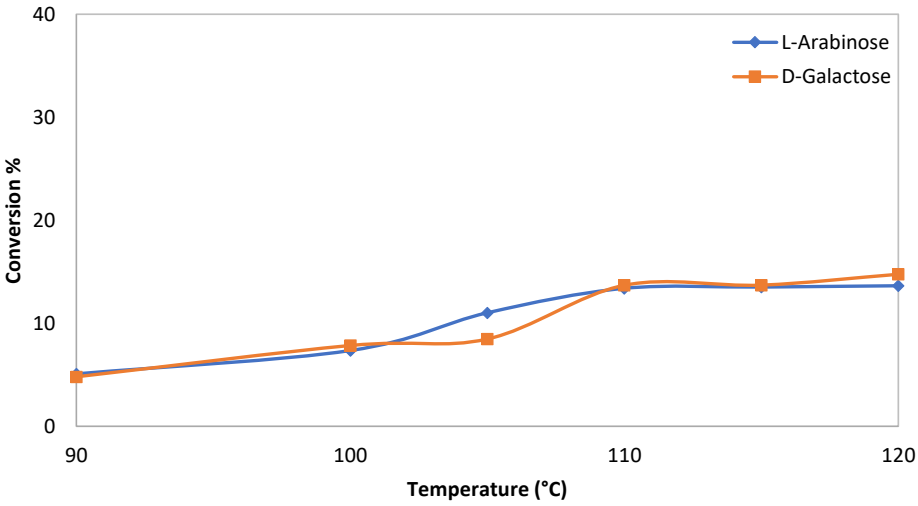

b)

Figure 14. Temperature effect on the conversion of a sugar mixture. Inlet molar ratio arabinose:galactose a) 1:1, b) 1:2.

The experiments demonstrated convincingly that it is possible to hydrogenate sugar mixtures on the solid foams (Figure 14). The system behaved in a stable manner and the sugars were converted to the corresponding sugar alcohols with a very high selectivity. This observation

has been confirmed by our previous studies of hydrogenation of binary sugar mixtures in slurry reactors in the presence of a ruthenium as the heterogeneous catalyst [8].

3.3. Residence time distribution and Péclet number

The residence time distribution (RTD) in the reactor system and in the solid foam structure was studied with step response experiments, which gave the cumulative distribution function $F(t)$. For a measurement signal $s(t)$ which is directly proportional to the tracer concentration ($s = a_0 + a_1 c$), the distribution function is calculated from

$$F(t) = \frac{s(t) - s_0}{s_\infty - s_0} \tag{1}$$

where s_0 corresponds the signal for zero concentration of the tracer and s_∞ is the asymptotic value of the signal. Numerical differentiation of the experimental data gives the density function of the RTD,

$$E(t) = \frac{dF(t)}{dt} \tag{2}$$

From $E(t)$, the mean residence time of the liquid ($\varepsilon_L \tau_L$) and the dimensionless variance (σ^2) are obtained as follows,

$$\varepsilon_L \tau_L = \int_0^\infty E(t) t dt \tag{3}$$

$$\sigma^2 = \int_0^\infty (t/(\varepsilon_L \tau_L) - 1)^2 E(t) dt \tag{4}$$

From the variance, the Péclet number is obtained as an iterative solution of the equation:

$$\sigma^2 = \frac{2}{Pe^2}(Pe - 1 + e^{-Pe}) \tag{5}$$

For large values of the Péclet number, the exponential term in equation (5) is negligible and a second-degree equation with respect to the Péclet number is obtained. The solution is straightforward,

$$Pe = \frac{1 + \sqrt{1 - 2\sigma^2}}{\sigma^2} \tag{6}$$

Figure 15 illustrates the $F(t)$ curves.

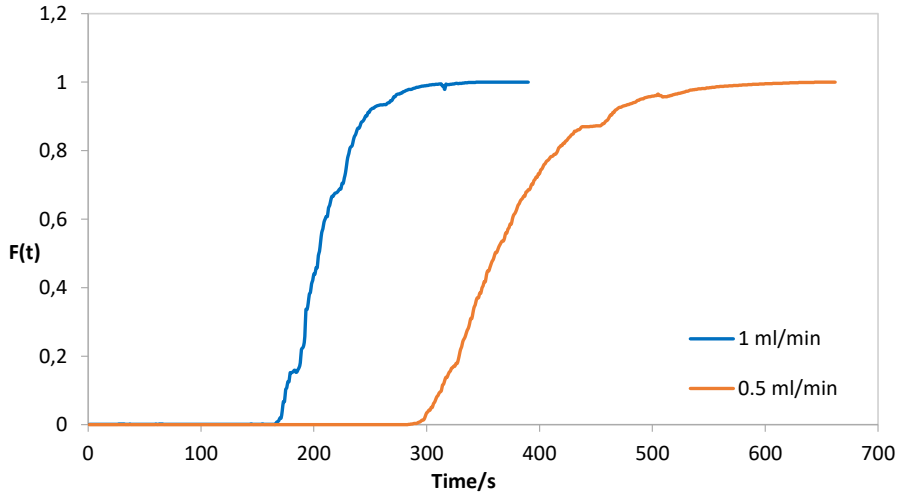

Figure 15. Cumulative distribution F(t) for two different liquid flow rates.

By numerical differentiation of the $F(t)$ curves, the $E(t)$ functions were obtained. The E curves at the gas superficial velocity 0.004 m/s are illustrated in Figure 16.

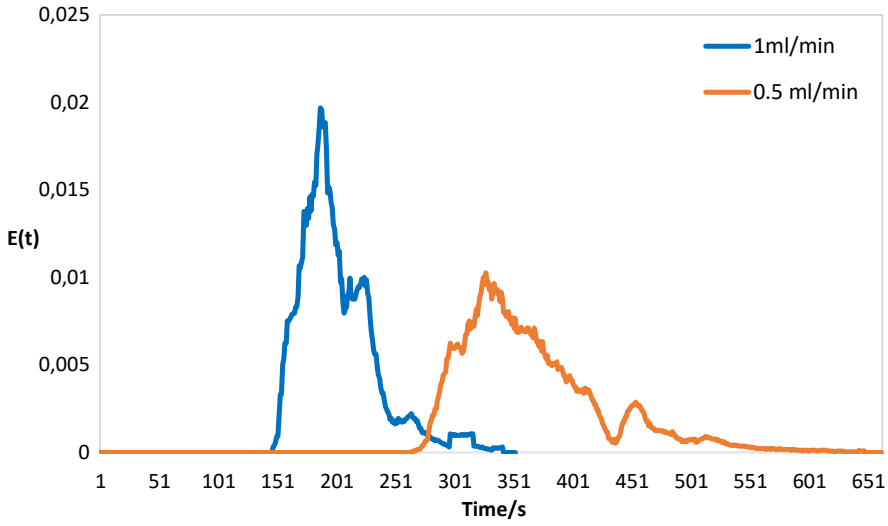

Figure 16. E(t) curve from the experiment for two different liquid flow rates.

Equations (3), (4) and (5) gave the mean residence time, the variance and the Péclet number, respectively. The results of the calculations are summarized in Table 3. Even though a signal

broadening is visible in the density function curves in Figure 16 so the variances are small, and consequently, the Péclet numbers are high, for the highest liquid flow rate (1 mL/min) the Péclet number exceeds 100.

Table 3. Results from RTD experiments.

F_G	mL/min	25.0	25.0
F_L	mL/min	0.5	1.0
$\varepsilon_L\tau_L$	/min – Eq. 3	376.7	209.6
σ^2	Eq. 4	0.0267	0.0194
Pe	Eq. 5	73.9	102.1

Because the RTD measurements indicated very high Péclet numbers, the estimation of kinetic parameters was done with the plug flow model ($Pe \rightarrow \infty$).

3.4. Kinetic model

3.4.1. Hypotheses on reaction mechanisms

The kinetic model was based on the hypothesis of a plausible reaction mechanism on the surfaces of ruthenium nanoparticles on the active carbon support. The following hypotheses were assumed to be valid for the reaction kinetics and thermodynamics. Sugar hydrogenation is known to be an irreversible reaction in practice; complete conversion of the reacting sugar to the corresponding sugar alcohol is reached, provided that the reaction time is long enough and an active catalyst is at disposal. This has been experimentally evidenced for the hydrogenation of glucose, arabinose, galactose, maltose, xylose, lactose and rhamnose [2, 7, 15-19]. Thus, the aspect of the overall thermodynamics of the hydrogenation process is not an important issue and is discarded here.

In previous research [2, 7, 13, 15-19], it has been suggested that the adsorption of sugar molecules on the catalyst surface is rapid compared to the hydrogenation step on the surface. This hypothesis has been used to describe the hydrogenation kinetics of individual sugar monomers and sugar mixtures on nickel and ruthenium surfaces [9, 12-15]. The surface reaction between adsorbed sugar and hydrogen is presumed to be the rate determining step in the process, whereas desorption of the sugar alcohol from the catalyst surface is assumed to be

rapid compared to the surface reaction step. The details of the hydrogen and sugar adsorption on metal surfaces is still a matter of debate. Both dissociative and non-dissociative adsorption of hydrogen has been proposed, and the adsorption of the sugar molecules has been assumed to be either competitive or non-competitive with hydrogen. Competitive adsorption might be the first obvious hypothesis. On the other hand, the size difference between a sugar molecule and hydrogen is huge, suggesting that after the adsorption of the sugar molecule, some interstitial metal sites remain accessible for hydrogen adsorption. Based on this hypothesis, Mikkola et al. [7], and Salmi et al. [55], have proposed a semi-competitive adsorption model for sugar molecules and hydrogen. The fundamental idea of the model is that the maximum coverage of the sugar molecule on the metal surface is $\theta_{max}<1$, whereas hydrogen molecule or hydrogen atom can reach full coverage ($\theta_{max}=1$) on the surface. The ultimate limit of the semi-competitive adsorption model is non-competitive adsorption, where the sites for the adsorption of the sugar molecule and hydrogen are regarded to be completely separate.

For the sake of simplicity, the non-competitive adsorption model is used in the present work. Dissociative adsorption of hydrogen is presumed, but hydrogen is assumed to preserve its molecular identity in the surface reactions, so that two hydrogen atoms react with adsorbed sugar in the rate-determining surface reaction. This kind of adsorption behavior has been proposed, for example, for the hydrogenation of aromatic compounds on metal surfaces [60]. The adsorption of the reaction product, the sugar alcohol is neglected. This hypothesis has been confirmed by the previous work of Sifontes et al. [19]: the adsorption affinity of the sugar monomer is clearly higher than that of the corresponding sugar alcohol. The catalyst surface is assumed to be ideal in the sense that the adsorption isotherm of Irving Langmuir can be applied. In case of sugar mixtures, the adsorption of different sugar molecules is assumed to be competitive, but the mutual interaction between the adsorbed sugar molecules is neglected. The adsorption and hydrogenation of two sugar molecules (A= arabinose, G=Galactose) to sugar alcohols (A'= arabitol, G'=galactitol) are considered.

3.4.2. Reaction mechanism and rate equations

Based on the hypotheses presented in the previous section, the mechanism of sugar hydrogenation can be written as follows; * denotes an active surface site for sugar adsorption and *' is a site for hydrogen adsorption:

A + * = A*

A + * = A*

H_2 + 2*' = 2H*'

A* + 2H*' → A' + * + *'

G* + 2H*' → G' + * + *'

Application of the quasi-equilibrium hypothesis on the adsorption steps gives

$$c*_i = K_i c_i c*$$ (7)

where i=A or i=G. For the dissociative adsorption of hydrogen is obtained

$$c*'_H = \sqrt{K_H c_H}\, c*'$$ (8)

The site balances for sugar and hydrogen adsorption are

$$\sum c*_j + c* = c_0$$ (9)

$$\sum c*'_H + c*' = c_0'$$ (10)

where c_0 and c_0' denote the total concentrations of the adsorption sites available on the catalyst surface. After inserting the quasi-equilibrium expressions (Eq. 7) and (Eq. 8) in the site balances, the concentrations of vacant sites are obtained,

$$c* = \frac{c_0}{1+K_A c_A + K_G c_G}$$ (11)

$$c*' = \frac{c_0'}{1+\sqrt{K_H c_H}} \quad (12)$$

The rates of the irreversible surface reaction steps are

$$r_I = k_1 c*_A \, c*'^{\,2}_H \quad (13)$$

$$r_{II} = k_2 c*_G \; c*'^{\,2}_H \quad (14)$$

The expressions for $c*$ and $c'*$ are inserted in the rate equations which become

$$r_I = \frac{k_I c_A c_H}{(1+K_A c_A+K_G c_G)(1+\sqrt{K_H c_H})^2} \quad (15)$$

$$r_{II} = \frac{k_I c_G c_H}{(1+K_A c_A+K_G c_G)(1+\sqrt{K_H c_H})^2} \quad (16)$$

where the merged constants are defined by

$$k_I = k_1 K_A K_H c_0 c_0'^2 \quad (17)$$

$$k_{II} = k_2 K_g K_H c_0 c_0'^2 \quad (18)$$

For constant hydrogen pressure and saturation conditions prevailing, Eqs. (15) and (16) are simplified to:

$$r_I = \frac{k_I' c_A}{1+K_A c_A+K_G c_G} \quad (19)$$

$$r_{II} = \frac{k_{II}' c_G}{1+K_A c_A+K_G c_G} \quad (20)$$

because the term $c_H/(1+(K_H c_H)^{1/2})^2$ is constant during the experiment.

Based on the reaction stoichiometry, the production and consumption rates of the compounds are obtained as follows,

$$r_A = -r_I \quad (21)$$

$$r_{A'} = r_I \quad (22)$$

$$r_G = -r_{II} \quad (23)$$

$$r_{G'} = r_{II} \quad (24)$$

$$r_H = -r_I - r_{II} \quad (25)$$

3.4.3. Mass transfer effects

Very thin catalyst layers are used in solid foams (<<100 micrometer) and – in relative sense – sugar hydrogenation belongs to the category of slow reactions [7], which implies that the internal mass transfer in the catalyst pores is rapid compared to the hydrogenation kinetics. The Thiele modulus is small and the effectiveness factor is high, in reality very close to 1 for thin catalyst layers as confirmed by numerical simulations of the reaction-diffusion model by Sifontes et al. [13, 18]. Therefore, the reaction-diffusion model for the catalyst layer is not needed, because the concentrations of hydrogen, the sugar and the sugar alcohol inside the catalyst pores of the open foam are equal to the concentrations at the outer surface of the catalyst layer.

The external mass transfer from the liquid bulk to the catalyst surface causes a complication on the interpretation of the experimental data obtained with the parallel tubular reactor system. In order to reach sugar conversion, the residence time should be long enough, which means that low liquid velocities are used. The consequence is that the Reynolds number (*Re*) is low, and the Sherwood number (*Sh*) is also low [45]; low Sherwood number implies low values of the liquid-solid mass transfer coefficient. The situation is illustrated in Figure 17. Because of the relatively low sugar conversions and high hydrogen flow rates, the gas-liquid mass transfer is of secondary importance. All the experiments were conducted at a relatively low sugar conversion level under a high hydrogen flow, so it is reasonable to assume that the longitudinal gradient of dissolved hydrogen in the liquid phase was minor.

A local mass balance for an organic component in the vicinity of the solid catalyst surface can be written as

$$r_i \Delta m_{cat} + N_i \Delta A_P = 0 \tag{26}$$

where m_{cat} is the mass of catalyst in the infinitesimal reactor volume element (ΔV). The catalyst mass in the volume element can be expressed with the catalyst bulk density (ρ_B) and the volume of the volume element: $\Delta m_{cat} = \rho_B \Delta V$.

The outer surface area of the solid catalyst (ΔA_P) in the volume element is expressed by $\Delta A_P / \Delta V = a_P$, where a_P denotes the surface area-to-volume ratio. The mass balance can be written as

$$r_i \rho_B + N_i a_P = 0 \tag{27}$$

The flux (N_i) is expressed with the simplest possible expression based on the film theory and the law of Fick:

$$N_i = k_{Li}(c_{Li} - c_i) \tag{28}$$

where c_i denotes the concentration at the outer surface of the catalyst material and c_{Li} is the measurable concentration in the liquid bulk. After inserting Eq. 28 in Eq. 27, the mass balance takes the form:

$$c_i / c_{Li} - r_i \rho_B / (k_{Li} a_P c_{Li}) = 1 \tag{29}$$

which is valid for all the components in the system (i= H_2, A, G, A', G'). The non-linear equation system (Eq. 29) is solved iteratively with respect to the surface concentrations (c_i). The bulk-phase concentrations (c_{Li}) are locally known, because they are obtained from the bulk-phase mass balances as will be described in section 3.5.

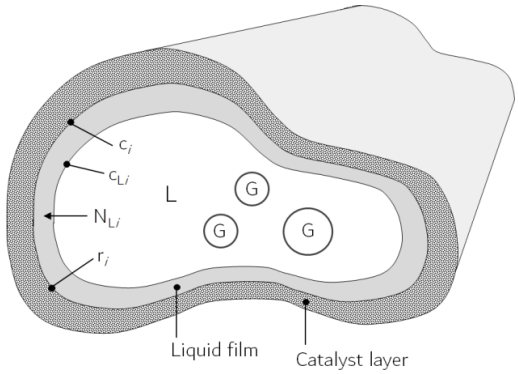

Figure 17. Modelling principle of external mass transfer and reaction in an open foam structure (P. Tolvanen).

3.5. Reactor modelling principles

3.5.1. Axial dispersion and plug flow models

The liquid-phase mass balances for the tubular reactor is based on the assumption of axial dispersion and plug flow in the open cell system in the foams, which was confirmed by studies of the residence time distribution in the reactor system. The dynamic form of the axial dispersion model was used to facilitate a robust numerical solution. Consequently, the mass balance for an arbitrary component (i) in the liquid phase can be written as

$$n'_{i,in} + (-D_i \frac{dc_i}{dl} A)_{in} = N_{i,} \Delta A_P + n'_{i,out} + (-D_i \frac{dc_i}{dl} A)_{out} + \frac{dn_{Li}}{dt} \quad (30)$$

which after introducing the differential elements becomes (out-in =Δ)

$$\Delta(D_i \frac{dc_i}{dl} A) - \Delta n'_i = N_{i,} \Delta A_P + \frac{dn_{Li}}{dt} \quad (31)$$

The cross-section area of the liquid phase is $A=\varepsilon_L \pi R^2$, where ε_L is the liquid volume fraction of the open cell structure. The surface area-to-reactor volume ratio (a_P) gives for the available surface area for mass transfer, $\Delta A_P / \Delta V = a_P$. The volume element is $\Delta V = \pi R^2 \Delta l$ Furthermore, assuming that the liquid flow rate is virtually constant, the molar flow can be expressed by $n'_i = c_{Li} w_L \pi R^2$, where w_L denotes the superficial velocity of the liquid. The

amount of substance in the volume element is $n_{Li} = c_{Li}\varepsilon_L \Delta V$. After combining this information and inserting the corresponding expressions in Eq. 31 and letting the length element $\Delta l \rightarrow 0$, the parabolic partial differential equation (PDE) is obtained ($z=l/L$),

$$\frac{dc_{Li}}{dt} = -\frac{w_L}{\varepsilon_L L}\frac{dc_{Li}}{dz} + \frac{D_i}{L^2}\frac{d^2c_{Li}}{dz^2} - N_{i,}a_P/\varepsilon_L \tag{32}$$

Equation (32) assumes that the axial dispersion coefficient is locally constant. After introducing the Péclet number and the residence time of the liquid phase, the final form of the model equation is obtained,

$$\frac{dc_{Li}}{dt} = -\frac{1}{\varepsilon_L \tau_L}\frac{dc_{Li}}{dz} + \frac{1}{Pe\tau_L}\frac{d^2c_{Li}}{dz^2} - N_{i,}a_P/\varepsilon_L \tag{33}$$

The model Eq. 33 is valid for both reactive and non-reactive conditions: for step-change experiments with inert tracers the interfacial flux (N_i) is set to zero.

The initial condition of the differential Eq. 33 is

$$c_{Li} = c_{Li}(0) \tag{34}$$

i.e. the concentration profiles inside the reactor tube are known in the beginning of the experiment.

For the reactor inlet and outlet, the closed boundary conditions of Peter Danckwerts [55], are applied,

$$c_{0Li} = c_{Li} - \frac{1}{Pe}\frac{dc_{Li}}{dz} \qquad \text{at } z=0 \tag{35a}$$

$$\frac{dc_{Li}}{dz} = 0 \qquad \text{at } z=1 \tag{35b}$$

For high Péclet numbers, plug flow conditions are approached, and the dispersion term in Eq. 33 becomes negligible and the boundary conditions (Eqs. 35 (a) and (b)) are replaced by the initial condition $c_{Li} = c_{0Li}$ at $z=0$. For steady-state conditions, the time derivative in Eq. 33 becomes zero and an ordinary differential equation (ODE) is obtained.

For the sake of comparison, the parameters of the axial dispersion model were determined by numerical simulation of the model, Eq. 33 where the flux term was set to zero (N_i=0) because the inert tracer did not interact with the foam. Similar results were obtained from the numerical simulation and the primary parameter estimation. The simulations with the experimental steps responses are compared in Figures 18 and 19 demonstrating the excellent fit of the axial dispersion model to the reactor system.

A further investigation of the flow pattern in the foam structure was performed by comparing two experiments: step responses from the entire reactor system (inlet region, feed section, foam and outlet region) with a stripped system, from which the foam was removed. The step responses from these experiments were almost identical, except a time delay obviously caused by the foam structure. The result implies that the signal broadening originates from the surrounding structure, whereas the foam itself provides almost plug flow conditions.

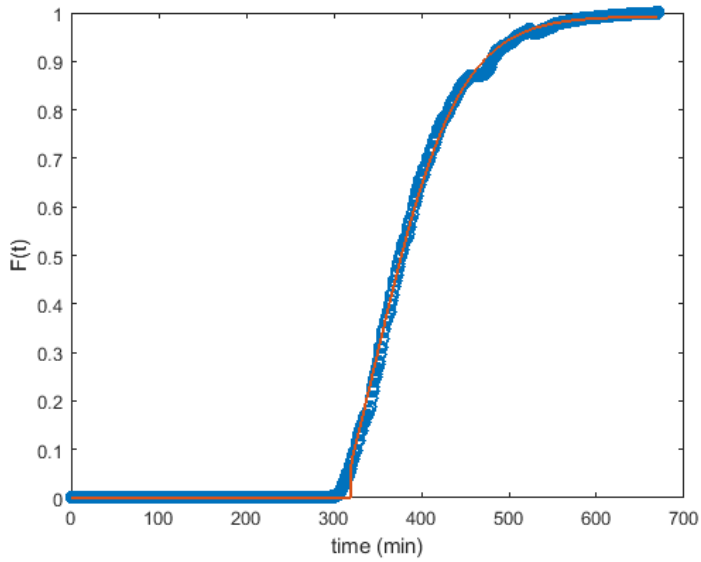

Figure 18. Fit of the axial dispersion model to the step response experiment (liquid flow rate 0.5 mL/min).

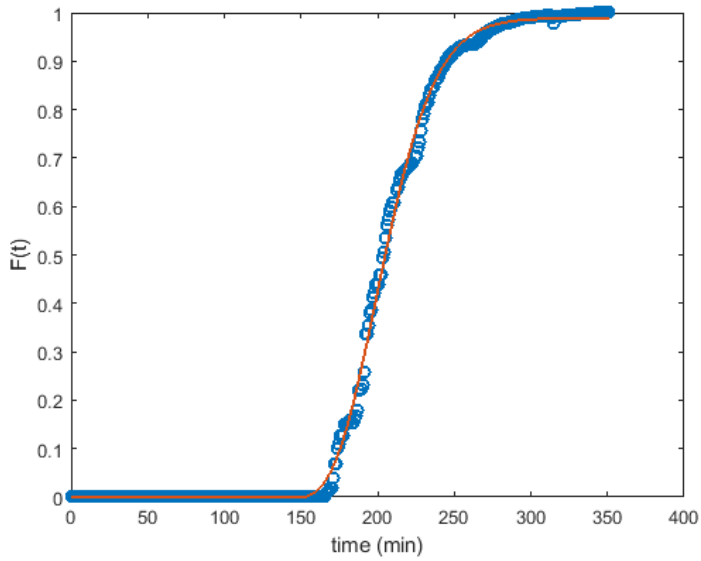

Figure 19. Fit of the axial dispersion model to the step response experiment (liquid flow rate 1.0 mL/min).

3.5.2. Summary of the general model – numerical aspects

The model consists of the rate equations (r_I and r_{II}, Eqs. (19) and (20)). The generation rates (r_i, Eqs. (21)-(25)), the mass transfer model (Eq. 29), as well as the reactor model with the initial and boundary conditions Eqs.33-35.

The following numerical strategy can be applied. The system of parabolic PDEs (Eq. 33) was discretized with finite differences for the dimensionless length coordinate (z). Backward differences should be used for the convection (plug flow) terms, the first derivatives, while central differences are used for the dispersion term, the second derivatives. The PDEs are in this way transformed to a large system of ODEs, an initial value problem, which is solved with an algorithm for stiff ODEs, the backward difference method of Henrici [56]. Inside the subroutine of the ODE solver, at each length coordinate, the mass transfer model (Eq. 29) should be solved iteratively to obtain the concentrations on the outer catalyst surface, which are needed in the calculation of the reaction rates.

During the estimation of the flow, rate and adsorption parameters, the ODE solver is operated under an optimization routine to find the optimal parameter values which minimized the objective function, i.e. residual sum of squares (Q),

$$\sum_i (c_{Li} - c_{Li,\exp})^2 \tag{36}$$

where the subscript 'exp' refers to the experimentally recorded concentrations. A hybrid simplex-Levenberg-Marquardt algorithm was used to minimize the objective function. The model was implemented to a modelling, simulation and estimation software ModEst [57].

3.6. Modelling results of hydrogenation kinetics and mass transfer

3.6.1 From the general model to simplifications

According to the residence time distribution measurements and modelling which resulted in very high Péclet numbers, the estimation of kinetic parameters was done with the plug flow model (Pe $\rightarrow\infty$). Moreover, the reaction dynamics was rather slow and most part of the experimental data was recorded under stationary conditions. Therefore the steady state version of the general model equation (33) was adopted.

The rate equations (Eqs. (19) and (20)) were the basis of the parameter estimation. The strong mutual correlation between the pre-exponential factor and activation energy is a serious problem in kinetic parameter estimation. This dilemma can partially be surmounted by an orthogonal transformation of the Arrhenius equation (i=A, i=G),

$$k_i = k_0 e^{-Eai/R(1/T-1/T0)} \tag{37}$$

where T_0 is the reference temperature (often the average temperature of the experiments) and k_0 is in fact the value of the rate constant at the average temperature. For the sake of simplicity and to avoid overparameterization of the estimation problem, the adsorption equilibrium parameters (K_A, K_G) were assumed to be independent of temperature.

After inserting the rate equations in the local balance equation at the catalyst surface (Eq. 29) for arabinose and galactose, the following expressions are obtained,

$$\frac{c_A}{c_{LA}} + \frac{\alpha_A c_A e^{-EaA/R(1/T-1/T0)}}{c_{LA}(1+K_A c_A + K_G c_G)} = 1 \tag{38}$$

$$\frac{c_G}{c_{LG}} + \frac{\alpha_G c_G e^{-EaG/R(1/T-1/T0)}}{c_{LG}(1+K_A c_A+K_G c_G)} = 1 \quad (39)$$

where the merged parameters, the dimensionless moduli are

$$\alpha_A = \frac{k_{0A}\rho_B}{k_{LA}a_P} \quad (40)$$

and

$$\alpha_G = \frac{k_{0G}\rho_B}{k_{LG}a_P} \quad (41)$$

However, parameters α_A and α_G are related. The liquid-phase mass transfer coefficient (k_{Li}) depends on the diffusion coefficient (D_i), typically k_{Li} is proportional to D_i,$^\gamma$ where γ=0.5…1. The film theory predicts γ=1, whereas the surface renewal theory of Danckwerts predicts γ=0.5. In many semi-empirical correlations values between 0.5 and 1 appear. Common correlations relate the Sherwood number to the Reynolds and Schmidt numbers [55], giving the proportionality of the mass transfer coefficient k_{Li} to the diffusion coefficient $D_i^{2/3}$.

The very frequently used correlation for the liquid-phase diffusion coefficient is the equation of Wilke and Chang [58],

$$D_i = \frac{\omega(\psi M)^{1/2}T}{{V_{mi}}^{0.6}\mu} \quad (42)$$

The symbols in Eq. 42 are defined in Notation. As the other parameters except the molar volumes at normal boiling point (V_{mi}) depend on the solvent only, the ratio of the diffusion coefficients of arabinose and galactose is easily obtained,

$$\frac{D_G}{D_A} = \left(\frac{V_{mA}}{V_{mG}}\right)^{0.6} \quad (43)$$

Consequently, assuming that k_{Li} is proportional to $D_i^{1/2\ldots2/3}$, we get

$$\frac{k_{LG}}{k_{LA}} = \left(\frac{V_{mA}}{V_{mG}}\right)^{0.3\ldots0.4} \quad (44)$$

The molar volumes of arabinose and galactose are calculated from the atomic increments of Le Bas according to the recipe provided by Reid et al. [59]. The molar volumes and ratios of diffusion and mass transfer coefficients are listed in Table 4.

Table 4. Molar volumes and ratios of diffusion and mass transfer coefficients.

i	V_{mi}	D_i/D_A	$\lambda=k_{Li}/k_{LA}$
Arabinose	148	1	1
Galactose	177.6	0.896	0.93…0.95

Atomic increments of Le Bas: C: 14.8, O: 7.4, H:3.7 [59].

The result implies that the mass transfer coefficient of galactose can be expressed with that of arabinose,

$$k_{LG} = \lambda k_{LA} \tag{45}$$

where λ=0.95..0.93 for the exponents 0.3…0.4 in Eq. 44 (Table 4) and Eqs. (38) and (39) become after introducing the dimensionless concentrations $y_A=c_A/c_{LA}$ and $y_G=c_G/c_{LG}$,:

$$y_A + \frac{\alpha_A y_A e^{-EaA/R(1/T-1/T0)}}{1+K_A c_{LA} y_A + K_G c_{LG} y_G} = 1 \tag{46}$$

$$y_G + \frac{\alpha_A y_G e^{-EaG/R(1/T-1/T0)}}{\kappa\lambda(1+K_A c_{LA} y_A + K_G c_{LG} y_G)} = 1 \tag{47}$$

where $\kappa=k_{0A}/k_{0G}$. The numerical solution of Eqs. (46) and (47) gives always y-values ≤1.

The simplified mass balances assuming plug flow and stationary state is for arabinose and galactose,

$$\frac{dc_{LA}}{dz} = -\frac{k_{0A}\rho_B c_{LA} y_A e^{-EaA/R(1/T-1/T0)}}{1+K_A c_{LA} y_A + K_G c_{LG} y_G}\tau_L \tag{48}$$

$$\frac{dc_{LG}}{dz} = -\frac{k_{0G}\rho_B c_{LG} y_G e^{-EaG/R(1/T-1/T0)}}{1+K_A c_{LA} y_A + K_G c_{LG} y_G}\tau_L \tag{49}$$

The model used for the estimation of kinetic parameters comprises Eqs. (48) and (49). During the parameter estimation, the dimensionless surface concentrations (y_A, y_G) of arabinose and galactose were solved iteratively from Eqs. (46) and (47) and inserted in the differential equations (Eqs. (48) and (49)), which were solved numerically with a backward difference algorithm of Henrici for stiff differential equations [54]. The objective function defined by Eq. 36 and the software ModEst was used in all the estimations [57].

3.6.2. Hydrogenation modelling results of sugar mixtures

The parameter estimation results are summarized in Tables 5-6 and the model predictions are compared with experimental data in Figures 20 and 21. In order to elucidate the effect of external mass transfer and to obtain the optimal model fit, the value of α_A was fixed to different values and the kinetic parameters were estimated by regression analysis. Then the degree of explanation (R^2) of different regression runs were compared. The results are shown in Table 5.

Table 5. Comparison of regression results for different values of α-parameter.

α_A	R^2
0	0.82
0.1	0.83
1	0.87
5	0.87
10	0.88
20	0.80
100	0.79

$$R^2 = 1 - \frac{\sum\left(c_{\exp} - c_{model}\right)^2}{\sum\left(c_{\exp} - c_{mean}\right)^2}$$

The conclusion is that the optimal α-value is around 10, which confirms the presence of external mass transfer limitation – an α-value 0 would imply intrinsic kinetic control. On the other hand, as the α-value vas increased, the degree of explanation started to decrease confirming the existence of an optimum. The final parameter estimation results along with the estimation statistics are presented in Table 6. The errors of the parameters were obtained from

the variances of the parameters, according to the table, the parameters are reasonably well estimated, most of them having the relative error less than 20%.

Table 6. Summary of parameter estimation results.

Parameter	Value	Error	Error/%
$k_{0A}\rho_B$ /min^{-1}	0.627E-02	0.114E-03	1.8
E_{aA} /Jmol^{-1}	0.868E+05	0.112E+05	13.0
$k_{0G}\rho_B$ /min^{-1}	0.635E-02	0.504E-03	7.9
E_{aG} /Jmol^{-1}	0.102E+06	0.172E+05	16.9
K_A /Lmol^{-1}	0.815E+02	0.162E+02	18.8
K_G / Lmol^{-1}	0.721E+01	0.478E+01	66.2

T_0= 378K (105°C), α=10, λ=0.94

The activation energies for arabitol and galactitol formation were 87 kJ/mol and 102 kJ/mol, respectively indicating that galactitol formation is favored at higher temperatures. The adsorption parameter was higher for arabinose than for galactose, which is expected because arabinose is a smaller molecule than galactose. The difference in the adsorption affinities of arabinose and galactose has previously been confirmed by Sifontes et al. [19], who carried out experiments with finely dispersed Ru/C slurries in a batch reactor.

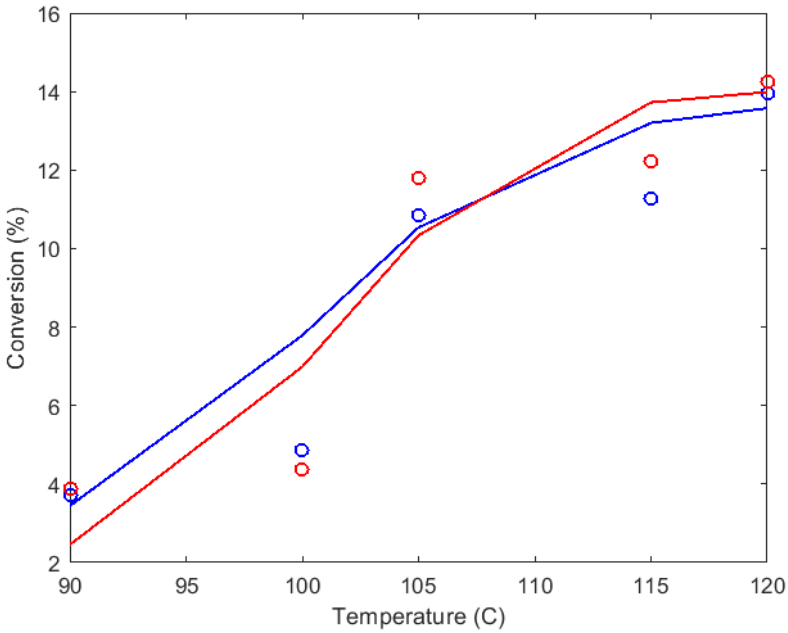

a)

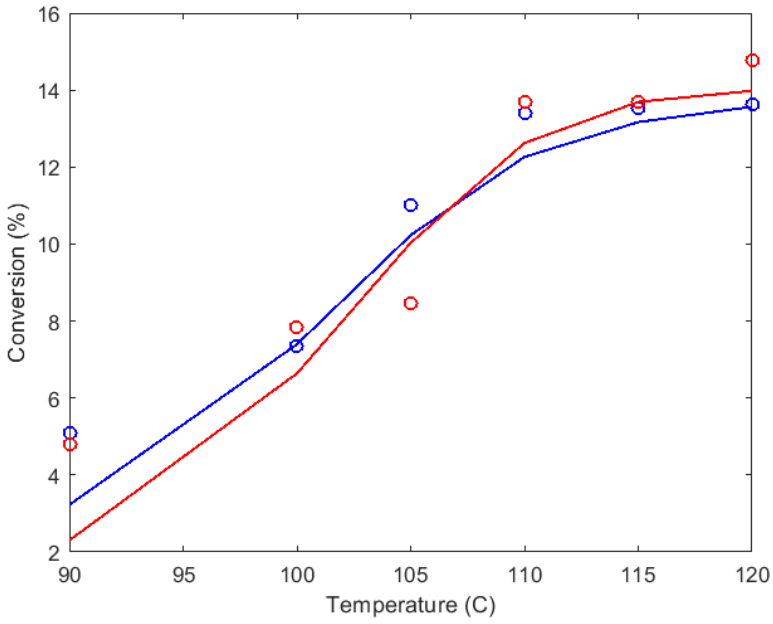

b)

Figure 20. Conversion of sugars at the reactor outlet at different temperatures (arabinose blue, galactose red). Inlet molar ratio arabinose:galactose a) 1:1, b) 1:2.

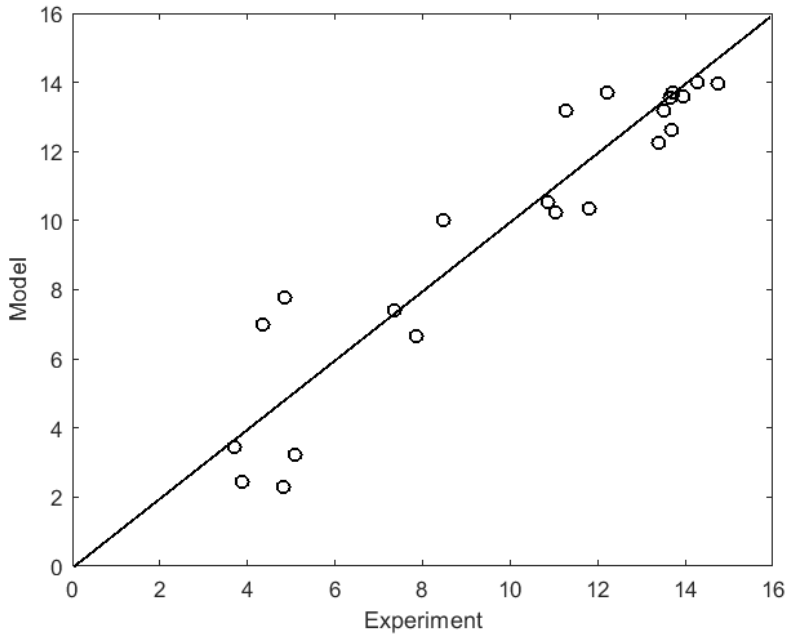

Figure 21. Parity plot of experimental data – comparison of experimental data and predictions.

An inspection of the numerical values of the dimensionless concentrations y_A and y_G (Eqs. (46) and (47)) gives information on the role of the external mass transfer resistance: in the absence of the mass transfer limitations, the *y*-values become 1 but in the presence of profound mass transfer limitations the value approach zero. This is clearly visible in the data provided in Table 7. At 90°C, the lowest experimental temperature, the *y*-values are around 0.8, but as the temperature increases the *y*-values are low, below 0.1. The retarding effect of mass transfer increases with temperature. The simulations confirm that neglecting the mass transfer effect would have given erroneous values of the activation energies.

From the value of the α_A parameter (Table 5) and the kinetic parameter $k_{0A}\rho_B$ (Table 6), the liquid-solid mass transfer parameter $k_{LA}a_P$ can be calculated using Eq. 30. According to Table 3, the optimal value of α_A is within the interval 1…10, which gives values $k_{LA}a_P$ =0.11…1.1*10^{-3} s^{-1}. In the literature references [41-44], values of gas-liquid mass transfer coefficients for solid foam structures are given and the orders of magnitude of the gas-liquid mass transfer coefficient for most of the previous literature discussed in ref. [44], are similar to our estimate of the liquid-solid mass transfer coefficient. It should however be emphasized that the comparison is not straightforward, because the solid foams are not exactly the same. To

obtain a value for the gas-liquid mass transfer coefficient for our system, separate mass transfer measurements under inert conditions, in the absence of chemical reactions would be needed.

Table 7. Dimensionless concentrations at the catalyst surface

Ratio	*T*/°C	y_A	y_G
A:G=1:1	*90*	0.7657	0.8142
	100	0.4513	0.4657
	105	0.2501	0.24
	115	0.0651	0.0504
	120	0.0382	0.0265
A:G=1:2	*90*	0.781	0.8271
	100	0.48	0.4945
	105	0.2716	0.2608
	110	0.1295	0.112
	115	0.0672	0.052
	120	0.0389	0.027

3.7. Models for continuous trickle bed reactor with open cell foam packing

Besides the intrinsic kinetics and flow pattern, the heat and mass transfer effects are critical issues in the mathematical modelling of solid foam structures. Heat and mass transfer resistance can appear at the gas-liquid interface, at the liquid-solid interface as well as inside the pores of the catalyst layer. The transport resistances at the gas-liquid and liquid-solid interfaces depend strongly on the flow conditions, i.e. on the Reynolds number. At low velocities the Reynolds number is low which implies that the Sherwood and Nusselt numbers are low and, consequently, the heat and mass transfer coefficients obtain low values. Many organic reactions applied in the production of fine and specialty chemicals and ingredients in alimentary products, are slow, which means that rather long residence times in the reactor are necessary to obtain a high conversion. Long residence times often imply low flow velocities in the reactor.

The impact of the internal mass transfer effects, on the other hand, depends on the ratio of the reaction and diffusion rates and the thickness of the catalyst layer. A common statement for catalytic processes carried out in structured reactors with thin catalyst layers (typically 50 micrometer or less) is that the internal mass transfer resistance in the catalyst pores is negligible. However, the role of internal mass transfer can become prominent even for thin catalyst layers if the chemical reaction is rapid and diffusion is slow. Therefore, two different

versions of the mathematical model are treated in detail in this study: a simplified model, where the gas-liquid and liquid-solid mass transfer resistance is considered and an advanced model, which includes the internal mass transfer resistance, too. Catalytic hydrogenation of sugars to sugar alcohols is taken as the case study. Because the experiments were carried out with dilute solutions of the sugars and the reaction enthalpy of sugar hydrogenation is moderate, the treatment is limited to isothermal cases. The system is schematically illustrated in Figure 22.

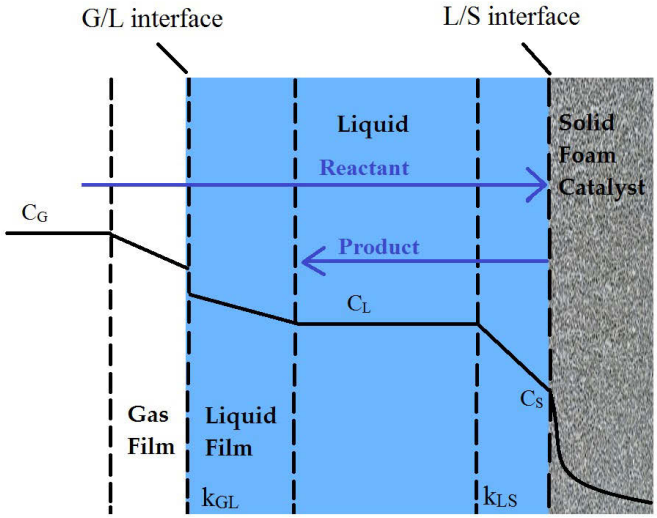

Figure 22. Interaction of kinetic and mass transfer effects in the tree-phase system: gas, liquid and solid foam catalyst.

Three-phase catalytic tubular reactor models were developed for solid foam packings. The unique feature of this model is that the gas, liquid and solid phase mass balances include most of the individual terms such as internal diffusion, gas-liquid and liquid solid mass transfer and intrinsic kinetics. Furthermore, the gas and liquid flows are described by axial and radial dispersion terms along with liquid hold-up and pressure drop expressions. Previous studies and review articles have been published for this kind of modeling approach for a trickle bed reactor (TBR) [45, 63-71]. We have developed a fast running two-dimensional (2D) model and gPROMS ModelBuilder version 5.1.1 (Process System Enterprise) was used for the implementation. Compared to models based on computational fluid dynamics (CFD) which demands heavy computations for multiple parameter estimation purposes [65-67], gPROMS provides fast computations and parameter estimation results at a reasonable time.

Two different versions of the mathematical model are presented in detail in this study: a simplified model, where the gas-liquid and liquid-solid mass transfer resistance is considered and an advanced model, which includes the mass transfer resistance in the catalyst pores. Time dependent concentrations and temperature at different locations (axial and radial position) inside the tubular reactor are acquired by solving the mass balances, kinetic rate laws, and fluid dynamic expressions simultaneously.

3.7.1. Simplified model

Time dependent concentrations and temperature at different locations (axial and radial position) inside the tubular reactor were acquired by solving mass balances, kinetic rate laws, and fluid dynamic expressions simultaneously. The gas-phase mass balance for a component (*i*) is shown in Eq. 50 including accumulation, gas-liquid mass transfer, convection, as well as axial and radial dispersion,

$$\varepsilon_G \frac{\partial C_{i,G}(t,z,r)}{\partial t} = -k_{GL}a_{GL}\left(C^*_{i,L} - C_{i,L}\right) - u_G \frac{\partial\left(C_{i,G}(t,z,r)\right)}{\partial z} + \varepsilon_G D_{z,G}(z,r)\left(\frac{\partial^2 C_{i,G}(t,z,r)}{\partial z^2}\right) + \varepsilon_G D_{r,G}(z,r)\left(\frac{\partial^2 C_{i,G}(t,z,r,)}{\partial r^2} + \frac{1}{r}\frac{\partial C_{i,G}(t,z,r,)}{\partial r}\right) \quad (50)$$

The mass balance for the liquid bulk phase, Eq. 51, shows that the accumulation equals a net effect of gas-liquid mass transfer, convection, as well as axial and radial dispersion. The liquid–solid mass transfer terms to supply reacting species from the liquid to the surface of the catalyst are included. The $k_{LS}a_{ls}\left(C_{i,L} - C_{i,s}\right)$ term describes the mass transfer of hydrogen and sugar (e.g. arabinose) from the liquid bulk to the catalyst surface and the mass transfer of product (e.g. arabitol) from catalyst surface to the liquid bulk.

$$\varepsilon_L \frac{\partial C_{i,L}(t,z,r)}{\partial t} = +k_{GL}a_{GL}\left(C^*_{i,L} - C_{i,L}\right) - k_{LS}a_{LS}\left(C_{i,L} - C_{i,S}\right) - u_L \frac{\partial\left(C_{i,L}(t,z,r)\right)}{\partial z}$$

$$+\varepsilon_L D_{z,L}(z,r)\left(\frac{\partial^2 C_{i,L}(t,z,r)}{\partial z^2}\right) + \varepsilon_L D_{r,L}\left(\frac{\partial^2 C_{i,L}(t,z,r)}{\partial r^2} + \frac{1}{r}\frac{\partial C_{i,L}(t,z,r)}{\partial r}\right) \quad (51)$$

Another mass balance is required for the liquid film surrounding the catalyst layer in order to calculate concentrations of the liquid at the catalyst surface. This mass balance only includes the liquid–solid mass transfer and the reaction terms. A quasi-steady state is presumed to prevail in the liquid film: the mass transfer is compensated by the chemical reaction,

$$k_{LSi}a_{LS}\left(C_{i,L} - C_{i,s}\right) + \rho_{cat}r_{effi}(t,z,r) = 0 \quad (52)$$

In general, the effective component consumption/production reaction rate is the intrinsic rate multiplied by the effectiveness factor:

$$r_{effi} = r_i\,\eta_{ei} \quad (53)$$

For thin catalyst layers and slow reactions η_{ei}=1 can be assumed and the concentration gradients inside the catalyst layer are negligible. If the internal mass transfer in the pores of the catalyst layer has an impact on the observed kinetics, the effectiveness factor is obtained from the general reaction-diffusion model of the catalyst layer as will be shown in Section 3.7.2.

3.7.1.1. Boundary conditions for the simplified model

The boundary conditions equations include the feed concentrations at the reactor inlet, as well as axial and radial derivatives of the component concentrations. The closed-closed boundary conditions of Danckwerts are applied at the reactor inlet and outlet. The boundary conditions are summarized below.

3.7.1.2. Gas-phase boundary conditions

$C_{i,G}^{IN} = C_{i,G}(t,r) - (\varepsilon_G D_{z,G}(z,r)/u_G)(dC_{i,G}(t,r)/dz)$ at z=0

Entrance (54a)

$\frac{\partial C_{i,G}(t,r)}{\partial z} = 0$ at z=L

Outlet (54b)

$\frac{\partial C_{i,G}(t,z)}{\partial r} = 0$ at r=0

Center (55a)

$\frac{\partial C_{i,G}(t,z)}{\partial r} = 0$ at r=R

Wall (55b)

3.7.1.3. Liquid-phase boundary conditions

$C_{i,L}^{IN} = C_{i,L}(\mathrm{t,r}) - (\varepsilon_L D_{z,L}(z,r)/u_L)(dC_{i,L}(\mathrm{t,r})/dz)$ at z=0 **Entrance** (56a)

$\frac{\partial C_{i,L}(t,r)}{\partial z} = 0$ at z=L **Outlet** (56b)

$\frac{\partial C_{i,\mathrm{L}}(t,z)}{\partial r} = 0$ at r=0 **Center** (57a)

$\frac{\partial C_{i,\mathrm{L}}(t,z)}{\partial r} = 0$ at r=R **Wall** (57b)

3.7.1.4. Summary of balance equations

The reactor model consists of the gas-phase balances (Eq. 50), the liquid-phase balances (Eq. 51), the surface balances (Eqs. (52) and (53)) as well as the boundary conditions (Eqs. (54)-(57)). The gas- and liquid-phase balances (Eqs. 50 and 51) are parabolic partial differential equations (PDEs) which are coupled to the surface balance (Eq. 52), which is a non-linear algebraic equation system (NLEs).

3.7.2. Advanced model

The simplified model presented in the previous section 3.7.1. is extended to a more advanced one by including the effect of the diffusion resistance inside the catalyst layer. This means that the mass balance equation (Eq. 52) will be replaced by a reaction-diffusion model for the porous catalyst layer.

3.7.2.1. Gas phase mass balance

The gas phase mass balance remains the same as stated by Eq.50.

3.7.2.2. Liquid phase mass balance

In the advanced model, it is assumed that reactions occur within the solid catalyst layer. Thus, reacting components are diffusing first into the solid catalyst layer and then react on the active surface sites of the catalyst. Intrinsic reaction kinetics, effective diffusivities of the molecules

inside the catalyst layer and the shape of the layer determine the net flux to/from the catalyst layer.

3.7.2.3. Mass transfer through the liquid film and in the pores of the catalyst layer

The component flux (*N*) through the liquid film around the catalyst material is (the component index '*i*' is left out for the sake of brevity)

$$NA = k_{LS}(c_L - c_{LS})A = D_{eff}\frac{dc_L}{dR}A \tag{58}$$

where A is the outer surface area of the catalyst in the reactor volume. The surface area is related to the number of catalyst elements and the surface areas of individual elements in the volume,

$$A = n_P A_P \tag{59}$$

For spherical particles is valid:

$$n_P A_P = n_P 4\pi {R_c}^2 \tag{60}$$

The catalyst bulk density is defined by

$$\frac{n_P V_P \rho_P}{V_R} = \frac{m_{cat}}{V_R} = \rho_B \tag{61}$$

which gives for the number of particles

$$n_P A_P = \frac{\rho_B V_R}{\rho_P V_P} A_P \tag{62}$$

For a spherical particle, the surface area-to-volume ratio is

$$\frac{A_P}{V_P} = \frac{3}{R_c} \tag{63}$$

This relation can be generalized to an arbitrary geometry by introducing the shape factor (s=0 for slabs, s=1 for long cylinders and s=2 for spheres),

$$\frac{A_P}{V_P} = \frac{s+1}{R_c} \tag{64}$$

Now the accessible mass transfer area can be expressed as

$$A = n_P A_P = \frac{\rho_B}{\rho_P}\left(\frac{s+1}{R_c}\right)V_R \tag{65}$$

The ratio $a=A/V_R$ is defined and the expressions above are inserted in the first equation (A1) which becomes

$$Na = k_{LS}(c_L - c_{LS})a = D_{eff}\frac{dc_L}{dR}\frac{\rho_B}{\rho_P}\left(\frac{s+1}{R_c}\right) \tag{66}$$

After introducing the dimensionless coordinate $x=R/R_c$ the relation

$$Na = k_{LS}(c_L - c_{LS})a = (s+1)\frac{\rho_B}{\rho_P}\left(\frac{D_{eff}}{{R_c}^2}\right)\frac{dc_L}{dx} \tag{67}$$

is obtained. The factor (f) is

$$f = (s+1)\frac{\rho_B}{\rho_P} \tag{68}$$

where f is a correction factor, typically f=1 or less for a structured catalyst.

Therefore, the liquid phase mass balance can be obtained from Eq. 69. Mass transfer flux to/from the catalyst layer is added on the very right-hand side of the correlation. The impact of such flux terms has been discussed in previous studies [71, 73, 74].

$$\varepsilon_l \frac{\partial C_{i,L}(t,z,r)}{\partial t} = +k_{GL}a_{GL}\left(C^*_{i,L} - C_{i,L}\right) - u_L\frac{\partial C_{i,L}(t,z,r)}{\partial z} + \varepsilon_L D_{z,L}\frac{\partial^2 C_{i,L}(t,z,r)}{\partial z^2}$$

$$+\varepsilon_L D_{r,L}\left(\frac{\partial^2 C_{i,L}(t,z,r)}{\partial r^2} + \frac{1}{r}\frac{\partial C_{i,L}(t,z,r)}{\partial r}\right) - \frac{f\,D_{eff,i}}{{R_C}^2}\left(\frac{\partial C_{i,s}(t,z,r,x)}{\partial x}\right)|x=1 \tag{69}$$

3.7.2.4. Porous catalyst layer

The foam properties are inbuilt in parameters such as D_{eff}, ε_p, R_C, and ρ_{cat} in solid phase mass balance, Eq. 70. A dimensionless coordinate, *x,* is taken in use, because the catalyst layer is typically very thin (<10 micrometer) and it is reasonable that the reactor and particle coordinates are not too different in the model implementation. The dimensionless coordinate is defined as $x=r_P/R_C$, where R_C is the catalyst layer thickness. Thus x is always between 0 and 1, where '1' corresponds to the outer surface of the catalyst layer.

$$\frac{\partial C_{i,s}(t,z,r,\mathrm{x})}{\partial t} = \frac{D_{eff,i}}{\varepsilon_p R_C^2}\left(\frac{\partial^2 C_{i,s}(t,z,r,\mathrm{x})}{\partial x^2} + \frac{s}{x}\frac{\partial C_{i,s}(t,z,r,\mathrm{x})}{\partial x}\right)$$

$$+\rho_{cat}\sum\left(\upsilon_{i,j} r_j(t,z,r,\mathrm{x})\right) \quad (70)$$

Due to the fact that the washcoat layer is very thin, the simple slab geometry can be used and then shape factor becomes 0. A shape factor, proposed by Bracconi et al. [72], equals to 0.475 for foams with circular strut cross-sectional shape and 0.810 for triangular shape. All three possibilities were considered in our modeling effort.

3.7.2.5. Liquid-phase boundary conditions

Also here, the boundary conditions of Danckwerts are applied at the reactor inlet and outlet,

$C_{i,L}^{IN} = C_{i,L}(\mathrm{t,r}) - (\varepsilon_L D_{z,L}(z,r)/u_L)(dC_{i,L}(\mathrm{t,r})/dz)$ at z=0 **Entrance** (71a)

$\frac{\partial C_{i,L}(t,r)}{\partial z} = 0$ at z=L **Outlet** (71b)

$\frac{\partial C_{i,\mathrm{L}}(t,z)}{\partial r} = 0$ at r=0 **Center** (72a)

$\frac{\partial C_{i,\mathrm{L}}(t,z)}{\partial r} = 0$ at r=R **Wall** (72b)

3.7.2.6. Solid-phase boundary conditions

For the porous catalyst layer, the particle balance is coupled to the bulk liquid balance through the boundary condition, which states that the molar flux through the liquid film is equal to the

molar flux in/out to/from the particle. This form is numerically stable even for the extreme case that $k_{i,LS}$ is large (i.e. no mass transfer limitation in the film surrounding the catalyst layer) and then $C_{i,s}$= $C_{i,L}$.

$$\frac{\partial C_{i,s}(t,z,r,\mathrm{x})}{\partial x} = 0 \text{ at x=0} \tag{73a}$$

$$C_{i,s} + \frac{D_{eff,i}}{k_{i,LS}} \frac{\partial C_{i,s}(t,z,r,\mathrm{x})}{R_C\, \partial x} = C_{i,L} \quad \text{at x=1 (outer surface of the layer)} \tag{73b}$$

3.7.2.7. Effectiveness factor

The effectiveness factor of a component is by definition the ratio between the diffusion flux to/from the porous particle under diffusion-influence conditions and under the conditions of intrinsic kinetics. The effectiveness factors of the components are obtained from the integrated local rates inside the particle,

$$\eta_{\mathrm{ei}} = \frac{(s+1)}{r_{\mathrm{i}}\,(c_{,\mathrm{L}})} \int_0^1 r_{\mathrm{i}} x^{\mathrm{s}} dx \tag{74}$$

where $r_{\mathrm{i}}(c_{,\mathrm{L}})$ denotes the rate calculated with the bulk-phase concentrations. The use of Eq. (74) minimizes the numerical inaccuracies in the evaluation of the effectiveness factors, because it is based on the use of the integrated rates over the entire catalyst layer [73, 74]. The effectiveness factor is obtained direct after that the particle model Eq. (70) has been solved.

3.7.3. Physical properties

The most important physical properties needed in the model are density, viscosity and hydrogen solubility. From the density and viscosity data, the liquid-phase diffusion coefficients can be calculated.

3.7.3.1. Hydrogen solubility

The hydrogen solubility in the liquid phase is calculated by the following empirical expression proposed by Rivero et al. [83] and Sifontes et al. [13]. The correlation equation (Eq.75) for the

hydrogen solubility is based on a large set of experimental data. The hydrogen pressure of the system is equal to P (bar), the temperature is T (K) and C_{H_2} (mol/L).

$$C_{H_2} = 9.35 \,.\, 10^{-6} \,.\, P_{H_2} \,.\, T + 0.01447 \,.\, 10^{-4} \,.\, T^2 - 1.138 \,.\, 10^{-3} \,.\, T + 0.222 - 2.833 \,.\, 10^{-3} \,.\, P_{H_2} - 0.1481 \,.\, 10^{-8} \,.\, {P_{H_2}}^2 \quad (75)$$

3.7.3.2. Liquid viscosity and molecular diffusivities

Eq. 76 was implemented for the dynamic viscosity of the liquid phase. It is dependent on both concentration of the sugar solution and temperature. This correlation proposed by Rivero et al. [83] and Sifontes et al. [13] is based on density and kinematic viscosity measurements of sugar solutions. T (K) is the temperature of the system and x_A is the weight fraction of the sugar in the solution (wt.%).

$$\mu_L[Pa.s] = \exp\left(\frac{1.54 x_A}{T_L - 273} + 3.81 \,.\, 10^{-4} \, x_A^2 - 1.10 \,.\, 10^{-2} \, x_A - 2.85 + \frac{1.94 \,.\, 10^2}{T_L - 273} - \frac{3.89 \,.\, 10^3}{(T_L - 273)^2}\right) \,.\, 10^{-3} \quad (76)$$

The molecular diffusivities of sugars, sugar alcohols and hydrogen in the liquid phase were calculated by using the Wilke and Chang correlation [58]:

$$D(m^2/s) = 7.4 \,.\, 10^{-12} \, \frac{(xM)^{0.5} \, T}{\mu \, V_A^{0.6}} \quad (77)$$

3.7.3.3. Gas and liquid densities

For the gas density, the ideal gas law is used. In the work of Rivero et al. [83] and Sifontes et al. [13], equations based on experiments with aqueous arabinose mixtures at different temperatures are given and can be applied here. T(°C) is the temperature of the system and x_A is the concentration of the solution (wt.%).

$$\rho\left[\frac{kg}{m^3}\right] = -0.008154 \,.\, \mathrm{T} \,.\, x_A + 0.008424 \,.\, {x_A}^2 + 4.797 \,.\, x_A + 1065 - 1.627 \,.\, T + 0.005412 \,.\, T^2 \quad (78)$$

3.7.4. Mass transfer coefficients

Under the actual experimental conditions, the liquid flow rate through the catalyst foam was low, which inevitably implies that the results are affected by the external mass transfer resistance at the outer surface of the foam. Therefore, correlations for mass transfer coefficients were considered and implemented in the model.

3.7.4.1. Gas-liquid mass transfer coefficient

A correlation for gas-liquid mass transfer coefficient in open-cell foam bed packing has been proposed by Zapico et al. [43],

$$\frac{a_{GL}\varepsilon_L}{a_p} Sh = 0.0037 Re_L^{1.4}\, Sc_L^{0.5} \tag{79}$$

where the Sherwood number is $\mathrm{Sh} = d_p k_{GL} D_L^{-1}$ and k_{GL} is the gas-liquid mass transfer coefficient.

It is reported in the literature that in packed bed reactors, the global mass transfer coefficient is expected to increase with the liquid superficial velocity but to show a small variation with the superficial velocity of the gas. A similar trend has been reported for packed beds with open cell foams [43, 75-77].

3.7.4.2. Liquid-solid mass transfer coefficient

The liquid-solid mass transfer coefficient (k_{LS}) was calculated by using Eq. 80 proposed by Cognet et al. [82],

$$k_{LS} = \left[Re_{L_{eq}} . \tau . Sc_L^{1/3} - 16.9 \cdot \frac{d_{hyd}}{d_R} Re_{L_{eq}}{}^{\beta} \cdot Sc_L^{1/3}\right] \cdot \frac{D_L}{d_{hyd}} \tag{80}$$

β = 0.28 for a 20 PPI foam and β = 0.25 for a 45 PPI foam was proposed by Lali et al. [84].
τ is the tortuosity of the foam structure and was calculated applying Eq. 81 which was proposed by Plessis et al. [86] :

$$\frac{1}{\tau} = \frac{3}{4\varepsilon} + \frac{\sqrt{9-8\varepsilon}}{2\varepsilon} \cdot cos\left\{\frac{4\pi}{3} + \frac{1}{3}cos^{-1}\left[\frac{8\varepsilon^2-36\varepsilon+27}{(9-8\varepsilon)^{1.5}}\right]\right\} \quad (81)$$

An alternative formula for the calculation of k_{LS} has been proposed by Mohammed et al. [62] for tubular reactors with solid foam packings,

$$\frac{\varphi Sh}{Sc^{1/3}} = aRe_L{}^b \, Re_G{}^c \left(a_s d_w \frac{1-\varepsilon}{\varepsilon}\right)^d \quad (82)$$

3.7.5. Liquid- holdup

The conditions of our experiments (very low gas and liquid superficial velocities) corresponded to the trickle flow regime as confirmed by the information available in the previous literature [75, 79-80]. To calculate the total liquid hold-up, as well as the static and dynamic hold-ups were estimated from Eqs. (83) and (84). Both correlations were proposed by Zalucky et al. [78], for solid foams. The dynamic holdup is based on the Galileo and Reynolds numbers while the static holdup is based on the Eötvös number.

$$\varepsilon_{L,dyn} = 4.44 Re_L^{0.56} \cdot Ga_L^{-0.42} \quad (83)$$

$$\varepsilon_{L,S} = \frac{1}{2.62+3.72 \cdot E\ddot{o}^*} \quad (84)$$

where the Eötvös number ($E\ddot{o}^*$) is

$$E\ddot{o}^* = \frac{\rho_L \cdot g \cdot d_e^2}{\sigma_L} \quad (85)$$

and the Galileo number (Ga_L) is : $Ga_L = \frac{g d_e^3}{v_L^2}$ (86)

3.7.6. Axial and radial dispersion coefficients

Saber et al. [42] have proposed a correlation for the Péclet number (Pe) in open cell foams. The concept was based on the use of the cell diameter (d_c). The Péclet number to calculate the axial dispersion coefficient is obtained as follows

$$Pe'_L = \frac{u_L d_c}{D_{z,L}} \tag{87}$$

where d_c= cell diameter, equivalent particle diameter.

$$Pe'_L = aRe^b \tag{88}$$

where a=0.042, b=0.5 for open cell foams according to Hochman and Effron [81]. The Péclet number used in the axial dispersion model is based on the reactor length,

$$Pe_L = \frac{u_L L}{D_{z,L}} \tag{89}$$

and we get

$$Pe_L = \frac{Pe'_L L}{d_c} \tag{90}$$

Finally, the axial dispersion coefficient is calculated from

$$D_{z,L} = u_L \frac{L}{Pe_L} \tag{91}$$

For the gas-phase axial dispersion coefficient, an analogous treatment is possible, giving

$$D_{z,G} = u_G \frac{L}{Pe_G} \tag{92}$$

The corresponding radial dispersion coefficient can be taken as a fraction of the axial one. As reported by Truong et al. [85], solid foam packing shows similar behavior of packed beds. Russo et al. [71], proposed that the value of radial dispersion coefficient is one third of the axial one for packed bed reactors. As a matter of fact, radial dispersion for systems not very much deviating from ideality are less influent than axial dispersion. A sensitivity analysis was conducted on this parameter, observing that its influence is only secondary on the simulation results.

3.7.7. Pressure drop

The experimental procedure of the pressure drop measurements is reported in Section 2.5. The following correlation for the estimation of the pressure drop in a tubular reactor with open cell foam packing has been proposed by Mohammed et al. [61] and it was used in this work:

$$\frac{dP}{dz} = \rho_L g(a_1 Re_L^{b_1} Re_G^{c_1})(a_s d_w \frac{1-\varepsilon}{\varepsilon})^{d_1} \quad (93)$$

where d_w = window (pore) diameter, a_1= 21.56, b_1= 0.15, c_1= 3.45, d_1= 9.80

3.7.8. Modeling results and discussion

3.7.8.1. Pressure drop results

The experimental and simulated data of pressure drop are compared in Figure 23. The simulations were based on Eq. 93.

In the existing literature, different characteristic lengths have been used for simulating the pressure drop. Saber et al. [42], used the cell diameter as a characteristic length, Mohammed et al., [61] used window diameter, and Edouard et al., [79] and Giani et al., [80] used the strut diameter. According to the experimental results obtained from the pressure drop measurements (Figures 23 and 24), we used the cell diameter as a characteristic length for simulating the pressure drop and the liquid hold up.

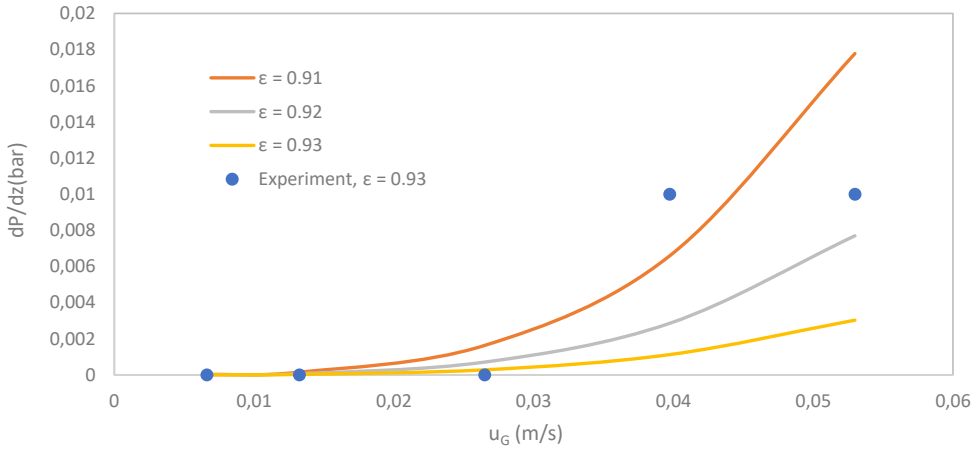

Figure 23. Experimental pressure drop data vs. simulations with different foam porosities.

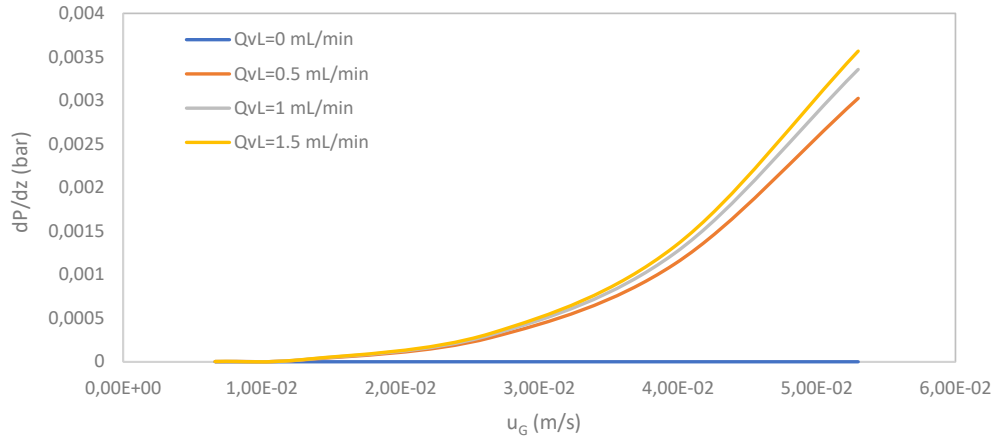

Figure 24. Experimental pressure drop data with different gas and liquid superficial velocities.

The experimental and simulated data of pressure drop are compared in Figure 23. The simulations were based on Eq. 93. The pressure drop experiments were conducted with carbon coated aluminum foams at the liquid volumetric flow rate of 0.5 ml/min and different gas volumetric flow rates (0-302 ml/min). The results display that changing the foam porosity has a strong effect on the pressure drop. An aluminum foam with a porosity of 0.93 was used for preparing the carbon coated foam catalyst. Comparing the experimental data with the simulation results indicates that the foam porosity was decreased to 0.916 because of the coating. Figure 24 displays the pressure drop experiments with different liquid (0.5-1.5 ml/min) and gas (0-302 ml/min) volumetric flow rates. The trends are expected.

3.7.8.2. Sugar mixtures hydrogenation results

The dynamic models presented in section 3.7 were implemented to describe the sugar mixtures (arabinose and galactose) hydrogenation experiments carried out in a trickle bed with a cylindrical solid foam packing as a case study. The geometric features listed in Table 8 were adopted from Amberosio et al. [84] as they used the same aluminum open cell foam, and the washcoat thickness layer value was adopted from Lali et al. [85] as they carried out the same method for coating aluminum open cell foams as we applied.

Figure 25 displays arabinose and galactose conversions as a function of temperature for experimental and calculated data for both simplified and advanced models. Both models were

capable to predict the conversions successfully. Hydrogenation experiments of binary sugar mixtures were performed with inlet molar ratios of 1:1 and 1:2. Experiments were carried out with liquid flow rate of 0.5 mL/min and gas (hydrogen) flow rate of 25 ml/min at different temperatures 90-120°C. The experimentally recorded sugar conversions on the figures are averages from multiple samples. The selectivity toward sugar alcohols was always very high, typically exceeding 95%.

Table 8. Geometrical properties of open cell foam with 0.93 porosity.

$* d_c\ [mm]$	$* d_w\ [mm]$	$* S_V\ [m^{-1}]$	$* d_S\ [mm]$	Washcoat thickness [µm]
1.85	0.95	954	0.2	~ 7

*Values were adopted from Amberosio et al. [84].

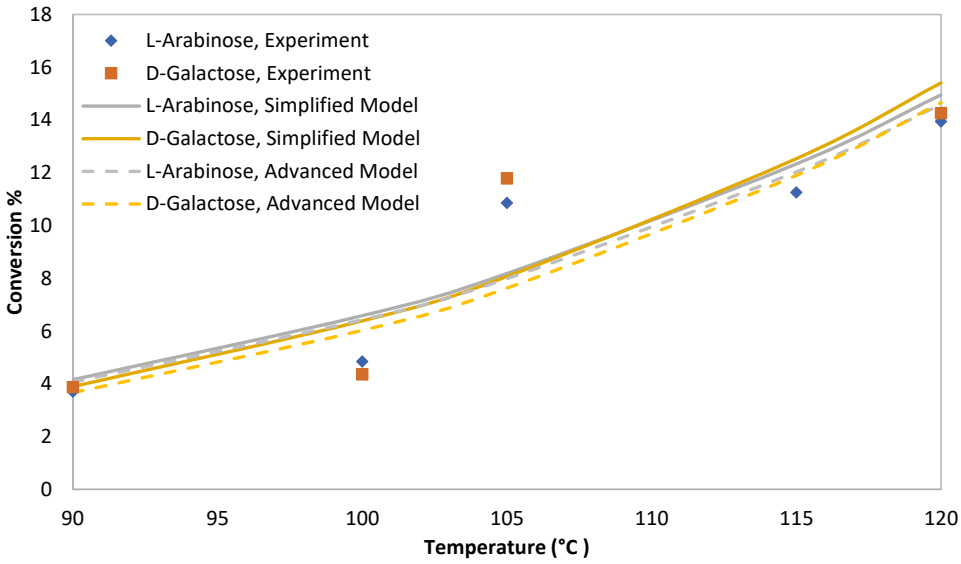

a)

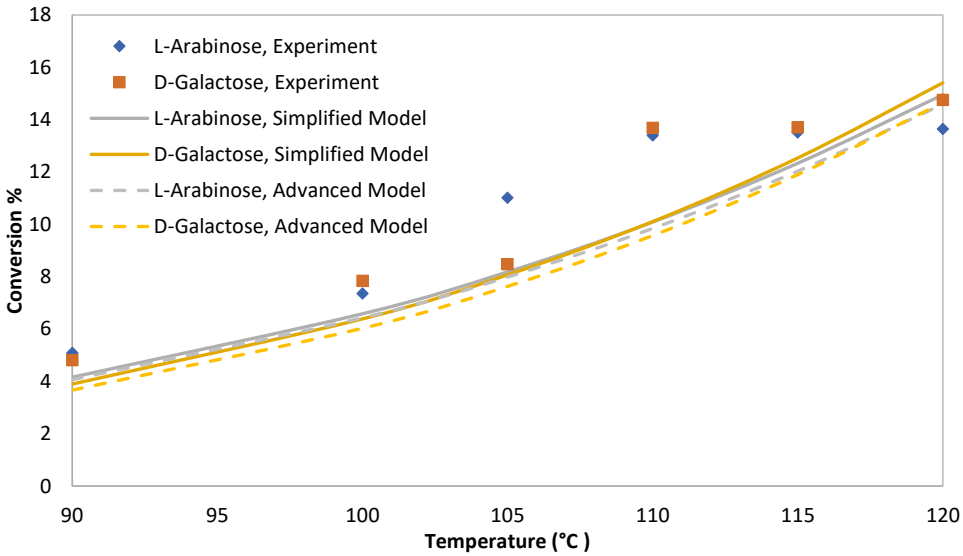

b)

Figure 25 Conversion of sugar mixtures as a function of temperature. Inlet molar ratio a) 1:1, b) 1:2.

3.7.8.3. Parameter estimation results and discussion

The parameter estimation results for both models including the activation energies and adsorption parameters with 95% confidence intervals are given in Tables 9 and 10. As revealed, in all cases the confidence intervals fall within 10% error, indicating a good accuracy of the parameters.

Table 9. Parameters estimation results for the simplified model.

Parameters	Estimated Value	95% Confidence Interval
$E_{a\,I}$ [J/mol]	5.36 E+04	3.57 E+03
$E_{a\,II}$ [J/mol]	5.76 E+04	4.07 E+03
k_{IrefA} s^{-1}	5.89 E-07	2.03 E-08
k_{IrefG} s^{-1}	5.81 E-07	2.05 E-08

Table 10.. Parameters estimation results for the advanced model with different shape factors (s).

Parameters	Estimated Value s=0	95% Confidence Interval	Estimated Value s=0.475	95% Confidence Interval	Estimated Value s=0.81	95% Confidence Interval
$E_{a\,I}$ [J/mol]	5.51 E+04	4.00 E+03	5.33 E+04	3.86 E+03	5.33 E+04	3.25 E+03
$E_{a\,II}$ [J/mol]	5.58 E+04	3.80 E+03	5.77 E+04	4.58 E+03	5.77 E+04	3.97 E+03
k_{IrefA} s^{-1}	5.76 E-07	2.20 E-08	8.77 E-07	3.27 E-08	1.12 E-06	3.57 E-08
k_{IrefG} s^{-1}	6.05 E-07	2.00 E-08	8.36 E-07	3.29 E-08	1.08 E-06	3.74 E-08

Corresponding parity plots for both models (the advanced and simplified ones) are displayed in Figure 26. There are good agreements between calculated (both models) and experimental data. The average error for the parity plots was about 16 %.

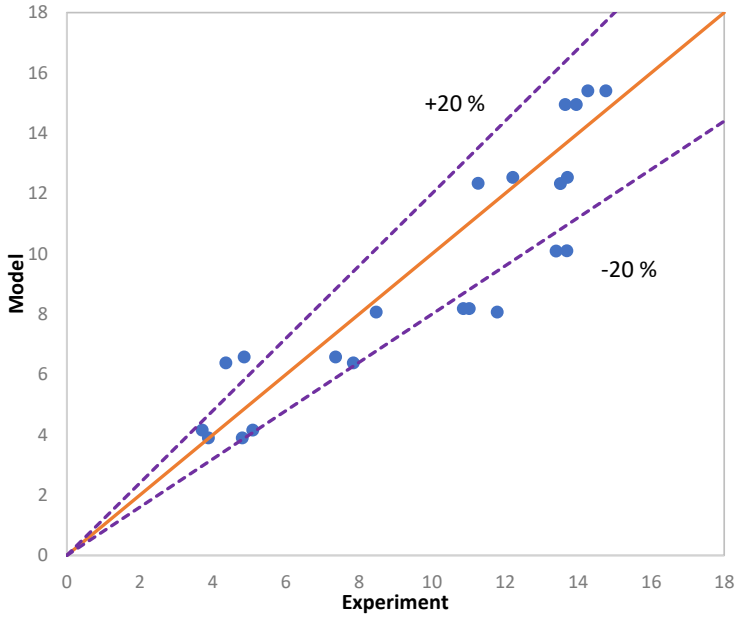

a)

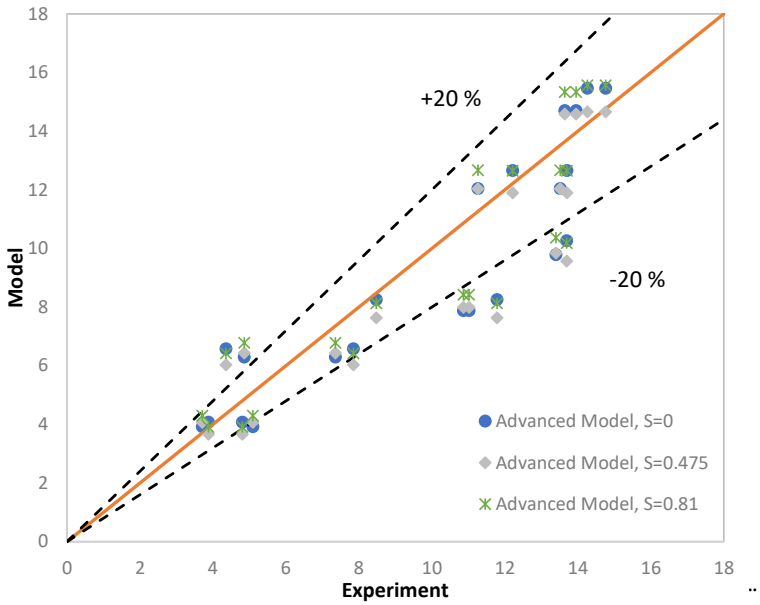

Figure 28. Parity plots of experimental data – simplified (a) and advanced model (b).

In Figures 29 and 30, the sugar mixture conversions and reaction rates along both the reactor length and radius are visualized. No conversion and reaction rate gradients appeared in the radial direction, and the gradients are virtually linear with the length of the reactor, which can be explained with the relatively low conversions in the tubular reactor.

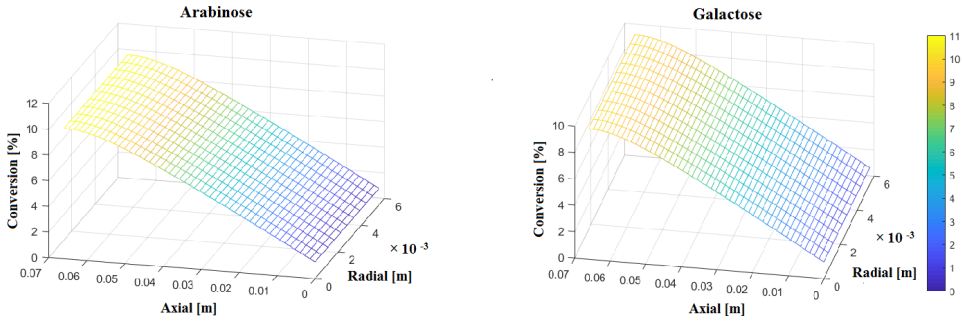

Figure 29. Arabinose and galactose conversions in axial and radial directions.

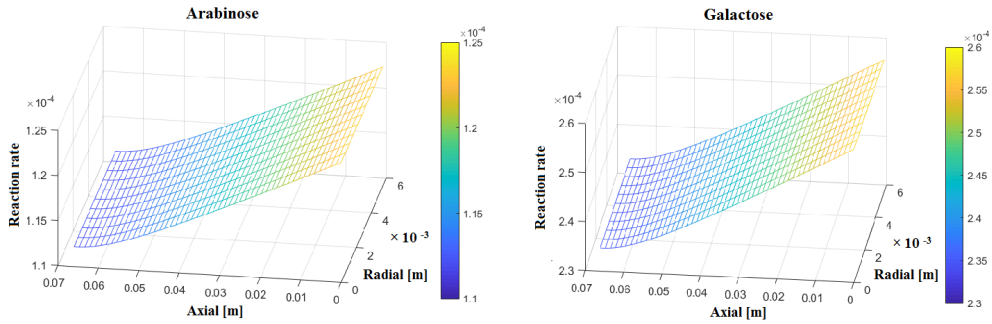

Figure 30. Reaction rates of sugar mixtures.

3.7.8.4. Sensitivity analysis

To examine the capabilities of our models, a sensitivity analysis was performed and the effect of the kinetic parameters and operation conditions on the arabinose and galactose conversions was studied. Figure 31 shows the effect of different kinetic parameters such as activation energy (E_a) and rate constant at the reference temperature (k_{Iref}) on the conversion of the sugar mixtures. As expected, the sugar conversion increased with increasing the activation energy and reference rate constant. The trends are rather linear. In the first case, starting from a sugar conversion of 10%, it is possible to improve it to 18% increasing 100% times the kinetic constant or the space time in the reactor. The results indicate that the sugar conversions had a higher dependence on the reference rate constant than on the energy of activation.

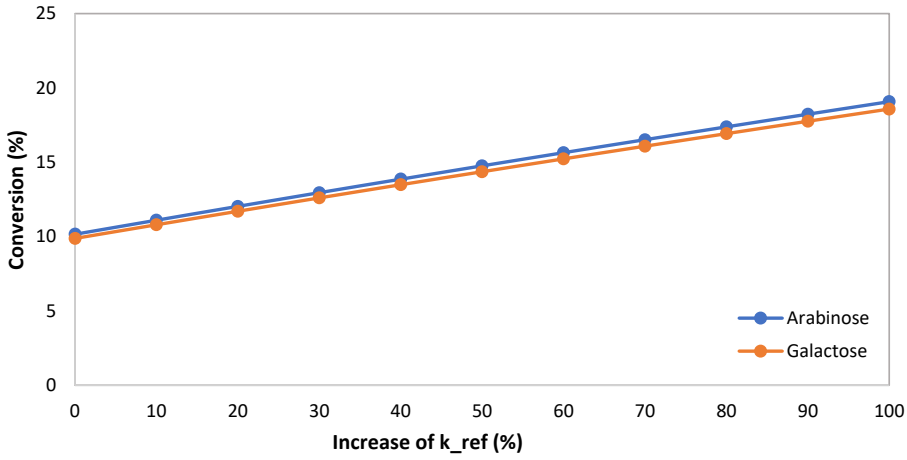

a)

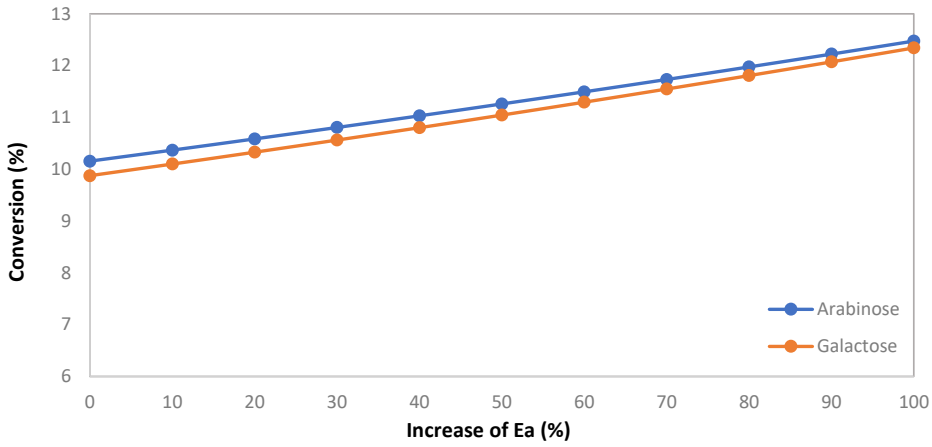

b)

Figure 31. Conversions of sugars as a function of the reference rate constant (a) and activation energy (b) with a washcoat thickness of 7 µm.

The effect of increasing the reference rate constant on the arabinose and galactose concentrations was studied in the middle and at the end of the reactor. The catalyst layer thickness of 600 µm was used as an example and results are displayed in Figures 32 and 33. The results show that as the reference rate constant increases, the concentrations of arabinose and galactose at the catalyst surface decrease which consequently results in an increase of the concentration gradient in the catalyst layer. This result surely demonstrates that the proposed model is very flexible, as it can simulate both ideal cases, characterized by a catalyst effectiveness factor approaching to the unity, and systems dominated by high intraparticle diffusion limitations. This aspect is surely a point of strength in the model utilization also for other chemical systems.

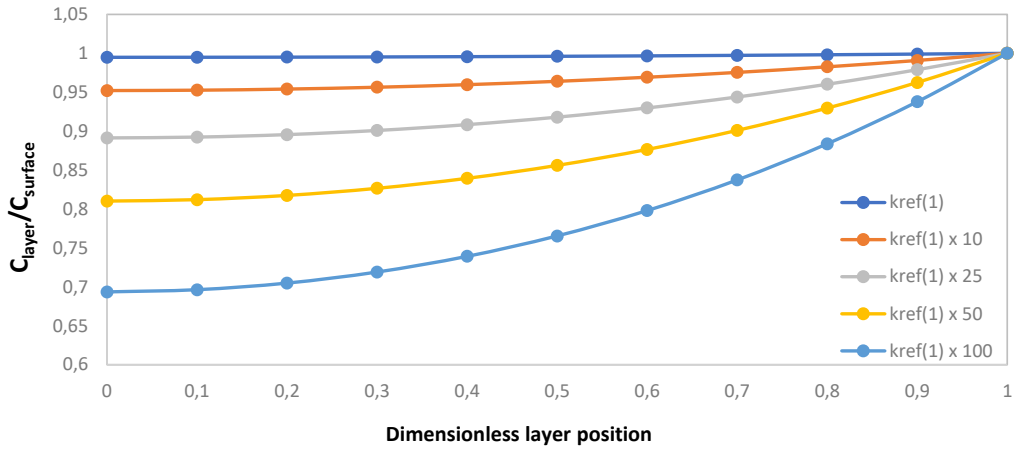

a) Arabinose concentration profiles in the washcoat in the middle of the reactor.

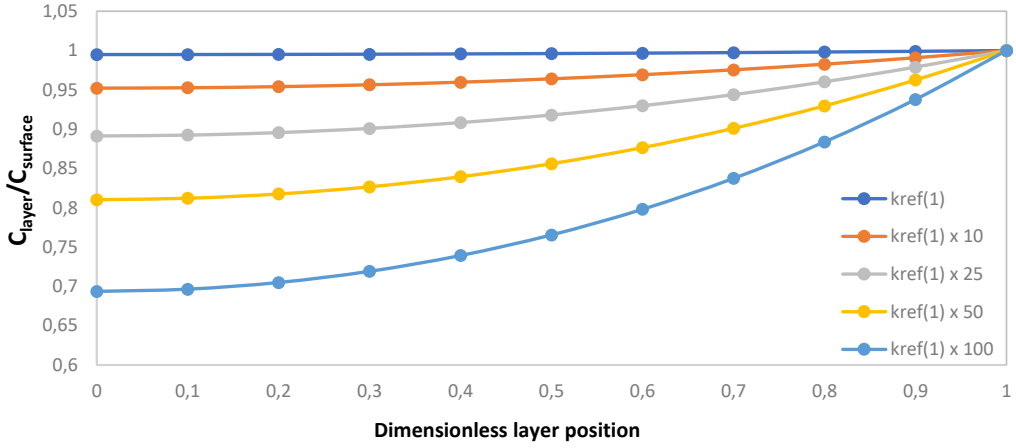

b) Arabinose concentration profiles in the washcoat at the reactor outlet.

Figure 32. Effect of increasing the reference rate constant on the arabinose concentrations in the middle of the reactor (a) and at the end of the reactor b) with washcoat thickness of 600 μm.

The effects are better highlighted by displaying a dimensionless concentration vs the layer position. In this way, at the catalyst surface, the dimensionless concentration is always less or equal to 1.

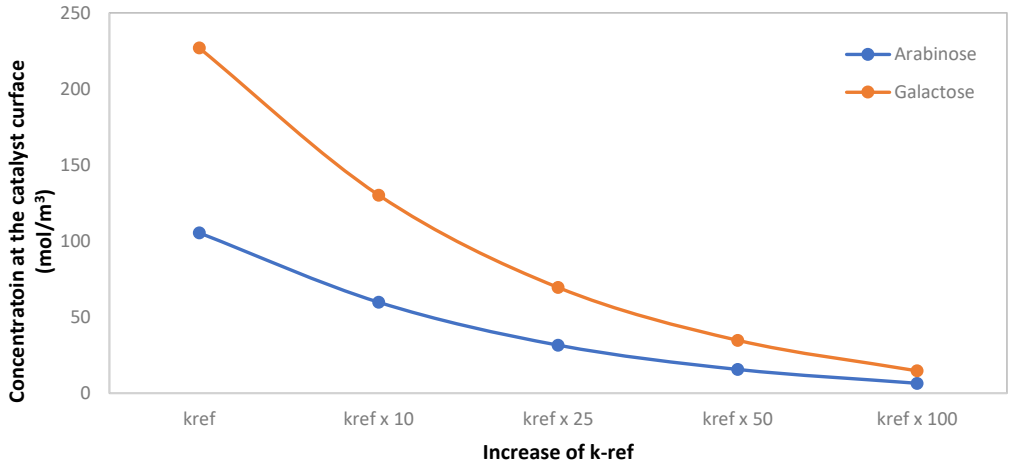

Figure 33. Arabinose and galactose surface concentrations in the middle of the reactor.

Figure 33 shows the calculated profiles at the catalyst surface, showing a decreasing value with the increase of the reference kinetic constant.

The effect of increasing the reactor length on the sugar conversions was studied in Figure 34, which shows that the conversions increased in line with the reactor length. No radial gradients are predicted even for longer reactors. The conversions as a function of the liquid flow rate and the inlet temperature are illustrated in Figure 35. The conversions increased strongly as the temperature increased and they were at its highest with low flow rates such as 0.5 ml/min. The results indicate that for obtaining higher conversions with a small reactor volume like the one we used in our experimental studies, it is better to use low liquid flow rates and high temperatures.

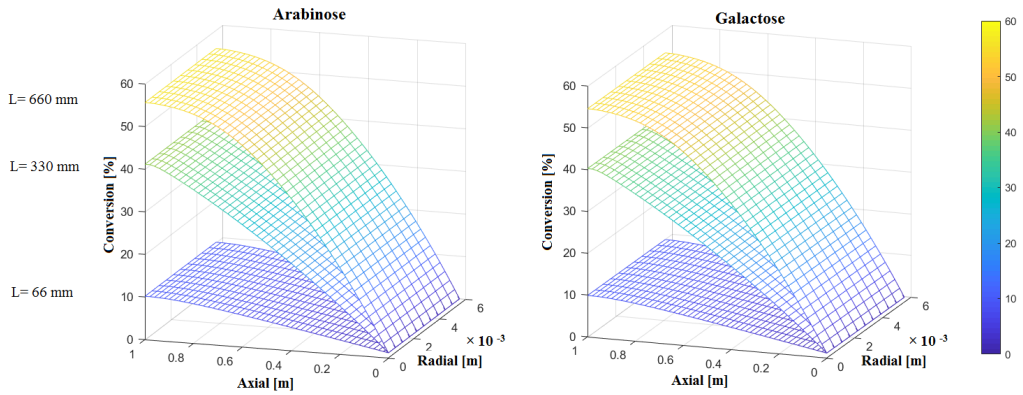

Figure 34. Conversions of arabinose and galactose as a function of the reactor length.

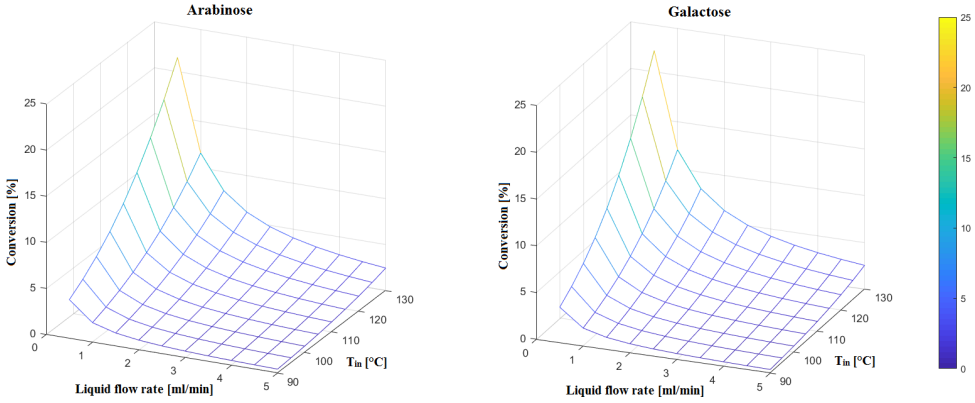

Figure 35. Conversions of arabinose and galactose as a function of the liquid flow rate and inlet temperature.

According to Figures 25-35, the model for the solid foam proposed in section 3.7. was capable of predicting the effect of different kinetic and transport phenomena under various operation conditions.

4. Conclusions

This work was carried out to develop structured catalyst and reactor technology for continuous production of sugar alcohols and to propose new advanced mathematical models for tubular reactors packed with solid foam catalysts.

Ruthenium-carbon based structured catalysts were developed and characterized to demonstrate the feasibility of the open-foam catalyst technology in the continuous and selective hydrogenation of sugar monomers and sugar mixtures to sugar alcohols. An active carbon support was prepared on open-cell aluminum foams. To incorporate a carbon layer into the aluminum foams, polymerization of furfuryl alcohol was performed. The incorporation of ruthenium on the carbon coated aluminum foams was implemented by homogeneous deposition precipitation. To test the mechanical stability of carbon coated foams, they were rotated at high speed in distilled water for one hour. No sign of decay was detected which confirmed the mechanical stability of the foam catalysts.

Hydrogenation of glucose, L-arabinose and a mixture of L-arabinose and D-galactose were conducted on ruthenium catalysts supported by carbon-coated aluminum foams in a multiphase multi-tubular reactor set-up which had six tubular reactors working in parallel. Various reaction parameters, such as sugar concentration, temperature and flow rate were screened. Through investigation a variety of reaction parameters, the temperatures 100-110°C and flow rates 0.5-1 mL/min were found to be suitable conditions for sugar hydrogenation to sugar alcohols. All the experiments were investigated at 20 bar hydrogen pressure. The catalytic hydrogenation was successful, the experimental reproducibility was good and foam catalysts were stable. For example, the selectivity of sorbitol was 99% at 90 ºC and 95% at 100 ºC. High selectivities were achieved in the hydrogenation of arabinose and galactose, too: the strongly dominating products were arabitol and galactitol. The chemical stability of the catalyst was confirmed in prolonged experiments in the continuous reactor system.

Residence time distribution (RTD) measurements were carried out to determine the flow pattern of the reactor system. Because the RTD measurements indicated very high Péclet numbers, the estimation of kinetic parameters was done with the plug flow model. A kinetic model for sugar hydrogenation was fitted to the experimental data obtained from open foam ruthenium catalysts. The model was applied on the hydrogenation of arabinose, galactose and glucose in a laboratory-scale open foam catalyst bed. The catalyst surface was assumed to be ideal in the sense that the

adsorption isotherm of Irving Langmuir can be applied. The non-competitive adsorption model was used for the adsorption of sugars and hydrogen. A mathematical model for the open foam structured catalyst was developed based on the concept of axial dispersion as the flow pattern. The effect of external mass transfer was included in the model, because it is in practice impossible to completely eliminate the external mass transfer limitations in continuous operation of the shallow foam bed: in order to obtain a high enough liquid residence time, low liquid velocities have to be used. The model was able to reproduce the important features of the experimental observations, both for the flow pattern and the experimentally observed hydrogenation kinetics.

The general principles of the model can be applied on other systems consisting of three-phase reactions in solid open foam catalysts. However, in case of gas-liquid mass transfer resistance, the model should be extended to comprise the gas-phase mass balances, as well. Therefore, we developed a new advanced comprehensive and transient multiphase model which included most of the individual terms such as internal diffusion, gas-liquid and liquid solid mass transfer and intrinsic kinetics for solid foam packings.

Advanced dynamic isothermal models for three-phase catalytic tubular reactors with solid foam packings were developed and implemented. The gas, liquid and solid phase mass balances included the individual terms such as internal diffusion, gas-liquid and liquid solid mass transfer and intrinsic kinetics for solid foam packings. Two versions of the mathematical model were considered in detail: a simplified model, where the gas-liquid and liquid-solid mass transfer resistances were included and an advanced model, which included the mass transfer resistance in the pores of the catalyst layer. Previously obtained catalytic hydrogenation results of binary sugar mixtures (arabinose and galactose) were utilized in this modelling and simulation effort.

gPROMS ModelBuilder was used for the model development and implementation which provided rapid computations and parameter estimation results at a reasonable time. Parameter estimations for both models, including the activation energies and adsorption parameters were carried out. In all the cases, the confidence intervals of the parameters remained within 10% error, indicating a good accuracy of the parameters. To investigate the model performance, a sensitivity analysis was carried out and the effect of the kinetic parameters and the operation conditions on the arabinose and galactose conversions was studied in detail.

The sugar conversions increased strongly as the temperature increased and they were at its highest with low flow rates such as 0.5 ml/min. The results indicate that for obtaining higher conversions with a small reactor volume like the one we used in the experimental studies, it is better to operate at low liquid flow rates and high temperatures. The effect of increasing the reference rate constant on the arabinose and galactose concentrations was studied in the middle and at the end of the reactor. It was demonstrated that the proposed model is very flexible, as it can simulate both ideal cases, characterized by a catalyst effectiveness factor approaching to the unity, and systems dominated by high intraparticle diffusion limitations.

The mathematical models for the solid foam proposed in this work was capable of predicting the effect of different kinetic and transport phenomena under various operation conditions. The models described in this work are applicable for other three-phase studies in catalytic tubular reactors packed with solid foams.

5. Notation

a_p	Packing specific surface area [m^2/m^3]
a_{GL}	Volume-specific gas-liquid interfacial surface area [m^2/m^3]
a_{LS}	Mass transfer area between liquid phase and foam catalyst [m^2/m^3] $a_{LS} = a_S \cdot \varepsilon_L$
a_S	Volume-specific geometrical surface area of foam substrate [m^2/m^3]
C_i^*	Component *i* saturation concentration [mol/m^3]
$C_{i,\mathrm{ref}}^*$	Component *i* saturation concentration at reference pressure [mol/m^3]
$C_{i,j}$	Concentration of component *i* in phase *j* [mol/m^3]
$C_{i,j}^{\mathrm{IN}}$	Initial concentration of component *i* in phase *j* [mol/m^3]
$D_{\mathrm{eff},i}$	Effective diffusivity of component *i* in water [m^2/s]
$D_{i,j}$	Molecular diffusivity of *i* in phase *j* [m^2/s]
$D_{r,j}$	Radial dispersion coefficient of phase *j* [m^2/s]
$D_{z,i}$	Axial dispersion coefficient of phase *j* [m^2/s]
dc	Cell diameter [m]
ds	Strut diameter [m]
d_w	Window (pore) diameter [m]
d_{hyd}	Hydraulic diameter [m] $dhyd = 4\varepsilon a_S^{-1}$
deq	Corrected equivalent diameter [m]
E_a	Activation energy [J/mol]
$E\ddot{o}^*$	Modified Eötvös number [–]
f	Correction factor [–]
Fr_j	Froude number [–]
Ga_L	Galileo number [–]
i	Component *i*
j	Phase *j* = G (gas), L (liquid), p (particle)
k	Kinetic constant [$mol/(g_{cat}\ s)$]
K_A	Arabinose adsorption parameter [m^3/mol]
K_G	Galactose adsorption parameter [m^3/mol]
K_{H2}	Hydrogen adsorption parameters [m^3/mol]
k_{GL}	Gas liquid mass transfer coefficient for component *i* [s^{-1}]
k_{LS}	Liquid solid mass transfer coefficient for component *i* [s^{-1}]

k_{ref}	Kinetic constant at reference temperature [mol/(g_{cat} s)]
L	Reactor length [m]
P	Pressure [Pa]
Pe_L	Peclet Number of the phase *j* [–]
R	Reactor radius [m]
r	Radial location [m]
R_C	Catalyst layer thickness [µm]
Re_L	Reynolds number for the liquid phase [–] $Re_L = \frac{\rho_L u_L d_{eq}}{\mu_L}$
R_g	Ideal gas constant [J/(K mol)]
r_{eff}	Effective reaction *j* rate [mol/(g s)]
r_j	Reaction *j* rate [mol/(g s)]
r_p	Particle radial location [m]
S_V	Packing specific surface area [m^2/m^3]
s	Shape factor [–]
Sh	Sherwood number [–]
Sc_L	Schmidt number [–] $S_{cL=}\mu_j D_L^{-1} \rho_j{}^{-1}$]
t	Time [s]
T_j	Temperature of phase *j* [K]
T_{ref}	Reference temperature [378 K]
u_j	Velocity of the phase *j* [m/s]
V	Reactor volume [m^3]
V_P	Particle volume [m3]
We_j	Weber number of the phase j [–]
x	Dimensionless coordinate [–]
x_A	Arabinose initial concentration [wt.%]
z	Axial location [m]
	Greek symbols
ε_B	Hydraulic void fraction [–]
ε_j	Holdup of phase *j* [–]
$\varepsilon_{L,dyn}$	Dynamic liquid holdup [–]
$\varepsilon_{L,s}$	Static liquid holdup [–]
η	Effectiveness factor [–]

η_j	Viscosity of phase *j* [Pa s]
ρ_j	Density of phase *j* [kg/m^3]
ρ_{cat}	Catalyst concentration referred to liquid phase [kg/m^3]
ρ_{bed}	Catalyst bulk density [kg/m^3]
σ_L	Liquid surface tension [N/m]
σ^2	Variance [–]
τ	Tortuosity [–]
τ_L	Liquid residence time [s]
ψ	Association factor [–]
ω	Dimensionless parameter for kinetics and mass transfer [–]
	Abbreviations
A	Arabinose
A'	Arabitol
H_2	Hydrogen
dyn	Dynamic
G	Galactose
G'	Galactitol
HPLC	High performance liquid chromatography
PDE	Partial differential equation
NLEs	Non-linear algebraic equation system

6. Acknowledgements

The present work was financed by Finnish Cultural Foundation, Neste-Fortum Foundation and Rector of Åbo Akademi University (Ali Najarnezhadmashhadi) and Academy of Finland, Academy Professor grant 319002 (Tapio Salmi). The economic support is gratefully acknowledged.

7. References

[1] J. Sanders, E. Scott, R. Weusthuis, H. Mooibroek, Bio-Refinery as the Bio-Inspired Process to Bulk Chemicals, Macromolecular Bioscience. 7 (2007) 105–117.

[2] V.A. Sifontes Herrera, O. Oladele, K. Kordás, K. Eränen, J.-P. Mikkola, D.Yu. Murzin, T. Salmi, Sugar hydrogenation over a Ru/C catalyst, Journal of Chemical Technology & Biotechnology. 86 (2011) 658–668.

[3] A. Kirilin, J. Wärnå, A. Tokarev, D.Yu. Murzin, Kinetic Modeling of Sorbitol Aqueous-Phase Reforming over Pt/Al_2O_3, Industrial & Engineering Chemistry Research. 53 (2014) 4580–4588.

[4] A. Cybulski, J.A. Moulijn, Structured Catalysts and Reactors, CRC Press, Taylor & Francis Group, Boca Raton, FL, 2005.

[5] D. Murzin, O. Simakova, Biomass Sugars for Non-Fuel Applications, Royal Society of Chemistry, 2015.

[6] B.W. Hoffer, E. Crezee, P.R.M. Mooijman, A.D. van Langeveld, F. Kapteijn, J.A. Moulijn, Carbon supported Ru catalysts as promising alternative for Raney-type Ni in the selective hydrogenation of d-glucose, Catalysis Today. 79-80 (2003) 35–41.

[7] J.-P. Mikkola, H. Vainio, T. Salmi, R. Sjöholm, T. Ollonqvist, J. Väyrynen, Deactivation kinetics of Mo-supported Raney Ni catalyst in the hydrogenation of xylose to xylitol, Applied Catalysis A: General. 196 (2000) 143–155.

[8] V.A. Sifontes Herrera, F. Saleem, B. Kusema, K. Eränen, T. Salmi, Hydrogenation of l-Arabinose and d-Galactose Mixtures Over a Heterogeneous Ru/C Catalyst, Topics in Catalysis. 55 (2012) 550–555.

[9] N. Déchamp, A. Gamez, A. Perrard, P. Gallezot, Kinetics of glucose hydrogenation in a trickle-bed reactor, Catalysis Today. 24 (1995) 29–34.

[10] C. Eisenbeis, R. Guettel, U. Kunz, T. Turek, Monolith loop reactor for hydrogenation of glucose, Catalysis Today. 147 (2009) S342–S346.

[11] T. Kilpiö, A. Aho, D. Murzin, T. Salmi, Experimental and Modeling Study of Catalytic Hydrogenation of Glucose to Sorbitol in a Continuously Operating Packed-Bed Reactor, Industrial & Engineering Chemistry Research. 52 (2013) 7690–7703.

[12] A. Aho, S. Roggan, K. Eränen, T. Salmi, D.Y. Murzin, Continuous hydrogenation of glucose with ruthenium on carbon nanotube catalysts, Catalysis Science & Technology. 5 (2015) 953–959.

[13] V.A. Sifontes Herrera, D.E. Rivero Mendoza, A.-R. Leino, J.-P. Mikkola, A. Zolotukhin, K. Eränen, T. Salmi, Sugar hydrogenation in continuous reactors: From catalyst particles towards structured catalysts, Chemical Engineering and Processing - Process Intensification. 109 (2016) 1–10.

[14] A. Najarnezhadmashhadi, K. Eränen, S. Engblom, A. Aho, D. Murzin, T. Salmi, Continuous Hydrogenation of Monomeric Sugars and Binary Sugar Mixtures on a Ruthenium

Catalyst Supported by Carbon-Coated Open-Cell Aluminum Foam, Industrial & Engineering Chemistry Research. 59 (2020) 13450–13459.

[15] J.-P. Mikkola, T. Salmi, R. Sjöholm, Modelling of kinetics and mass transfer in the hydrogenation of xylose over Raney nickel catalyst, Journal of Chemical Technology & Biotechnology. 74 (1999) 655–662.

[16] J. Kuusisto, J.-P. Mikkola, M. Sparv, J. Wärnå, H. Heikkilä, R. Perälä, J. Väyrynen, T. Salmi, Hydrogenation of Lactose over Sponge Nickel CatalystsKinetics and Modeling, Industrial & Engineering Chemistry Research. 45 (2006) 5900–5910.

[17] J. Kuusisto, J. Mikkola, M. Sparv, J. Wärnå, H. Karhu, T. Salmi, Kinetics of the catalytic hydrogenation of d-lactose on a carbon supported ruthenium catalyst, Chemical Engineering Journal. 139 (2008) 69–77.

[18] V.A. Sifontes, D. Rivero, J.P. Wärnå, J.-P. . Mikkola, T.O. Salmi, Sugar Hydrogenation Over Supported Ru/C—Kinetics and Physical Properties, Topics in Catalysis. 53 (2010) 1278–1281.

[19] V. Sifontes Herrera, Hydrogenation of L-arabinose, D-galactose, D-maltose and L-rhamnose, Doctoral thesis, Åbo Akademi University, Turku/Åbo Finland, 187 p., 2012.

[20] A. Corma, S. Iborra, A. Velty, Chemical Routes for the Transformation of Biomass into Chemicals, Chemical Reviews. 107 (2007) 2411–2502.

[21] S. Dumitriu, Polysaccharides: Structural Diversity and Functional Versatility, Second Edition, CRC Press, 2004.

[22] C. Ban, S. Yang, H. Kim, D.H. Kim, Effect of Cu addition to carbon-supported Ru catalysts on hydrogenation of alginic acid into sugar alcohols, Applied Catalysis A: General. 578 (2019) 98–104.

[23] B. Chen, U. Dingerdissen, J.G.E. Krauter, H.G.J. Lansink Rotgerink, K. Möbus, D.J. Ostgard, P. Panster, T.H. Riermeier, S. Seebald, T. Tacke, H. Trauthwein, New developments in hydrogenation catalysis particularly in synthesis of fine and intermediate chemicals, Applied Catalysis A: General. 280 (2005) 17–46.

[24] A. Aho, S. Roggan, O.A. Simakova, T. Salmi, D.Yu. Murzin, Structure sensitivity in catalytic hydrogenation of glucose over ruthenium, Catalysis Today. 241 (2015) 195–199.

[25] P. Frontera, A. Macario, M. Ferraro, P. Antonucci, Supported Catalysts for CO_2 Methanation: A Review, Catalysts. 7 (2017) 59.

[26] E.P. Maris, W.C. Ketchie, V. Oleshko, R.J. Davis, Metal Particle Growth during Glucose Hydrogenation over Ru/SiO_2 Evaluated by X-ray Absorption Spectroscopy and Electron Microscopy, The Journal of Physical Chemistry B. 110 (2006) 7869–7876.

[27] P.A. Son, S. Nishimura, K. Ebitani, Production of γ-valerolactone from biomass-derived compounds using formic acid as a hydrogen source over supported metal catalysts in water solvent, RSC Advances. 4 (2014) 10525.

[28] Y. Nakagawa, M. Ishikawa, M. Tamura, K. Tomishage, Selective production of cyclohexanol and methanol from guaiacol over Ru catalyst combined with MgO, Green Chemistry. 16 (2014) 2197–2203.

[29] D.D. Laskar, M.P. Tucker, X. Chen, G.L. Helms, B. Yang, Noble-metal catalyzed hydrodeoxygenation of biomass-derived lignin to aromatic hydrocarbons, Green Chemistry. 16 (2014) 897.

[30] F. Lali, S. Gärtner, S. Haase, R. Lange, Preparation Method for Ruthenium Catalysts Supported by Carbon-Coated Aluminum Foams, Chemical Engineering & Technology. 38 (2015) 1353–1361.

[31] C. Chatterjee, F. Pong, A. Sen, Chemical conversion pathways for carbohydrates, Green Chemistry. 17 (2015) 40–71.

[32] T. Vergunst, F. Kapteijn, J.A. Moulijn, Preparation of carbon-coated monolithic supports, Carbon. 40 (2002) 1891–1902.

[33] K. Boomsma, D. Poulikakos, F. Zwick, Metal foams as compact high performance heat exchangers, Mechanics of Materials. 35 (2003) 1161–1176.

[34] L. Giani, C. Cristiani, G. Groppi, E. Tronconi, Washcoating method for Pd/γ-Al_2O_3 deposition on metallic foams, Applied Catalysis B: Environmental. 62 (2006) 121–131.

[35] M.V. Twigg, J.T. Richardson, Fundamentals and Applications of Structured Ceramic Foam Catalysts, Industrial & Engineering Chemistry Research. 46 (2007) 4166–4177.

[36] F. Glenk, T. Knorr, M. Schirmer, S. Gütlein, B.J.M. Etzold, Synthesis of Microporous Carbon Foams as Catalyst Supports, Chemical Engineering & Technology. (2010) NA-NA.

[37] S. Genna, F. Trovalusci, N. Ucciardello, V. Tagliaferri, Improving Performance of an Open Cell Aluminium Foam through Electro-Deposition of Nickel, Materials. 12 (2019) 133. H.

[38] P.W.A.M. Wenmakers, J. van der Schaaf, B.F.M. Kuster, J.C. Schouten, Enhanced liquid–solid mass transfer by carbon nanofibers on solid foam as catalyst support, Chemical Engineering Science. 65 (2010) 247–254.

[39] T. Knorr, A. Schwarz, B.J.M. Etzold, Comparing Different Synthesis Procedures for Carbide-Derived Carbon-Based Structured Catalyst Supports, Chemical Engineering & Technology. 37 (2014) 453–461.

[40] M. Monno, D. Negri, V. Mussi, P. Aghaei, G. Groppi, E. Tronconi, M. Strano, Cost-Efficient Aluminum Open-Cell Foams: Manufacture, Characterization, and Heat Transfer Measurements, Advanced Engineering Materials. 20 (2018) 1701032.

[41] C.P. Stemmet, J. Van Der Schaaf, B.F.M. Kuster, J.C. Schouten, Solid Foam Packings for Multiphase Reactors, Chemical Engineering Research and Design. 84 (2006) 1134–1141.

[42] M. Saber, T.T. Huu, C. Pham-Huu, D. Edouard, Residence time distribution, axial liquid dispersion and dynamic–static liquid mass transfer in trickle flow reactor containing β-SiC open-cell foams, Chemical Engineering Journal. 185-186 (2012) 294–299.

[43] R.R. Zapico, P. Marín, F.V. Díez, S. Ordóñez, Liquid hold-up and gas–liquid mass transfer in an alumina open-cell foam, Chemical Engineering Science. 143 (2016) 297–304.

[44] T.-S. Nguyen, Y. Swesi, D. Edouard, P. Fongarland, Platelet Millireactor Filled with Open Cell Foam-Supported Pt Nanoparticles for a Three-Phase Catalytic System, Industrial & Engineering Chemistry Research. 58 (2019) 9352–9361.

[45] T.O. Salmi, J.-P. Mikkola, J.P. Wärnå, Chemical Reaction Engineering and Reactor Technology, Second Edition, CRC Press, Boca Raton, Fl. 2019.

[46] Y. Peng, Properties of ceramic foam catalyst supports: one-dimensional and two-dimensional heat transfer correlations, Applied Catalysis A: General. 266 (2004) 235–244.

[47] W. Lu, C.Y. Zhao, S.A. Tassou, Thermal analysis on metal-foam filled heat exchangers. Part I: Metal-foam filled pipes, International Journal of Heat and Mass Transfer. 49 (2006) 2751–2761.

[48] F. Rodríguez-Reinoso, The role of carbon materials in heterogeneous catalysis, Carbon. 36 (1998) 159–175.

[49] D.B. Thakur, R.M. Tiggelaar, T.M.C. Hoang, J.G.E. Gardeniers, L. Lefferts, K. Seshan, Ruthenium catalyst on carbon nanofiber support layers for use in silicon-based structured microreactors, Part I: Preparation and characterization, Applied Catalysis B: Environmental. 102 (2011) 232–242.

[50] F.-C. Buciuman, B. Kraushaar-Czarnetzki, Preparation and characterization of ceramic foam supported nanocrystalline zeolite catalysts, Catalysis Today. 69 (2001) 337–342.

[51] M. Toebes, Impact of the structure and reactivity of nickel particles on the catalytic growth of carbon nanofibers, Catalysis Today. 76 (2002) 33–42.

[52] F. Lali, G. Böttcher, P.-M. Schöneich, S. Haase, S. Hempel, R. Lange, Preparation and characterization of Pd/Al2O3 catalysts on aluminum foam supports for multiphase hydrogenation reactions in rotating foam reactors, Chemical Engineering Research and Design. 94 (2015) 365–374.

[53] V. Benessere, A. De Roma, F. Ruffo, Carbohydrates as Building Blocks of Privileged Ligands for Multiphasic Asymmetric Catalysis, ChemSusChem. 1 (2008) 425–430.

[54] T. Salmi, D.Yu. Murzin, J.-P. Mikkola, J. Wärnå, P. Mäki-Arvela, E. Toukoniitty, S. Toppinen, Advanced Kinetic Concepts and Experimental Methods for Catalytic Three-Phase Processes, Industrial & Engineering Chemistry Research. 43 (2004) 4540–4550.

[55] P.V. Danckwerts, Insights into Chemical Engineering: Selected Papers of P.V. Danckwerts, Elsevier, 2013.

[56] P. Henrici, Discrete variable methods in ordinary differential equations, Wiley, New York, NY, 1962.

[57] H. Haario, ModEst – User's Guide, Profmath Oy, Helsinki, 2011.

[58] C.R. Wilke, P. Chang, Correlation of diffusion coefficients in dilute solutions, AIChE Journal 1 (1955) 264–270.

[59] R.C. Reid, J.M. Prausnitz, B.E. Poling, The properties of gases and liquids, McGraw Hill, New York NY, 1987.

[60] T. Salmi, S. Toppinen, T.-K. Rantakylä, J. Aittamaa, A heterogeneous reaction-diffusion model for the catalytic three-phase hydrogenation of mixtures of substituted aromatic molecules, 1st European Congress Chemical Engineering (ECCE-1) 1997, Firenze, Proceedings, 2947-2950.

[61] I. Mohammed, T. Bauer, M. Schubert, R. Lange, Hydrodynamic multiplicity in a tubular reactor with solid foam packings, Chemical Engineering Journal 231 (2013) 334–344.

[62] I. Mohammed, T. Bauer, M. Schubert, R. Lange, Liquid–solid mass transfer in a tubular reactor with solid foam packings, Chemical Engineering Science 108 (2014) 223–232.

[63] M.H. Al-Dahhan, F. Larachi, M.P. Dudukovic, A. Laurent, High-Pressure Trickle-Bed Reactors: A Review, Industrial & Engineering Chemistry Research 36 (1997) 3292–3314.

[64] F.S. Mederos, J. Ancheyta, J. Chen, Review on criteria to ensure ideal behaviors in trickle-bed reactors, Applied Catalysis A: General 355 (2009) 1–19.

[65] A. Atta, S. Roy, K.D.P. Nigam, A two-phase Eulerian approach using relative permeability concept for modeling of hydrodynamics in trickle-bed reactors at elevated pressure, Chemical Engineering Research and Design 88 (2010) 369–378.

[66] Z.V. Kuzeljevic, M.P. Dudukovic, Computational Modeling of Trickle Bed Reactors, Industrial & Engineering Chemistry Research 51 (2012) 1663–1671.

[67] Y. Wang, J. Chen, F. Larachi, Modelling and simulation of trickle-bed reactors using computational fluid dynamics: A state-of-the-art review, The Canadian Journal of Chemical Engineering 91 (2011) 136–180.

[68] S. Schwidder, K. Schnitzlein, A new model for the design and analysis of trickle bed reactors, Chemical Engineering Journal 207-208 (2012) 758–765.

[69] A. Iordanis, Mathematical Modelling of Catalytic Fixed Bed Reactors, PhD dissertation, University of Twente, Netherlands, 2002.

[70] K.C. Metaxas, N.G. Papayannakos, Kinetics and Mass Transfer of Benzene Hydrogenation in a Trickle-Bed Reactor, Industrial & Engineering Chemistry Research 45 (2006) 7110–7119.

[71] V. Russo, T. Kilpiö, M. Di Serio, R. Tesser, E. Santacesaria, D.Yu. Murzin, T. Salmi, Dynamic non-isothermal trickle bed reactor with both internal diffusion and heat conduction: Sugar hydrogenation as a case study, Chemical Engineering Research and Design 102 (2015) 171–185.

[72] M. Bracconi, M. Ambrosetti, M. Maestri, G. Groppi, E. Tronconi, A fundamental investigation of gas/solid mass transfer in open-cell foams using a combined experimental and CFD approach, Chemical Engineering Journal 352 (2018) 558–571.

[73] S. Toppinen, T.-K. Rantakylä, T. Salmi, J. Aittamaa, Kinetics of the Liquid-Phase Hydrogenation of Benzene and Some Monosubstituted Alkylbenzenes over a Nickel Catalyst, Industrial & Engineering Chemistry Research 35 (1996) 1824–1833.

[74] S. Toppinen, T.-K. Rantakylä, T. Salmi, J. Aittamaa, Kinetics of the Liquid Phase Hydrogenation of Di- and Trisubstituted Alkylbenzenes over a Nickel Catalyst, Industrial & Engineering Chemistry Research 35 (1996) 4424–4433.

[75] [32] F. Turek, R. Lange, Mass transfer in trickle-bed reactors at low Reynolds number, Chemical Engineering Science 36 (1981) 569–579.

[76] S. Goto, J.M. Smith, Trickle-bed reactor performance. Part I. Holdup and mass transfer effects, AIChE Journal 21 (1975) 706–713.

[77] J. Zalucky, M. Wagner, M. Schubert, R. Lange, U. Hampel, Hydrodynamics of descending gas-liquid flows in solid foams: Liquid holdup, multiphase pressure drop and radial dispersion, Chemical Engineering Science 168 (2017) 480–494.

[78] C.P. Stemmet, F. Bartelds, J. van der Schaaf, B.F.M. Kuster, J.C. Schouten, Influence of liquid viscosity and surface tension on the gas–liquid mass transfer coefficient for solid foam packings in co-current two-phase flow, Chemical Engineering Research and Design 86 (2008) 1094–1106.

[79] D. Edouard, M. Lacroix, C.P. Huu, F. Luck, Pressure drop modeling on solid foam: State-of-the art correlation, Chemical Engineering Journal 144 (2008) 299–311.

[80] L. Giani, G. Groppi, E. Tronconi, Mass-Transfer Characterization of Metallic Foams as Supports for Structured Catalysts, Industrial & Engineering Chemistry Research 44 (2005) 4993–5002.

[81] J.M. Hochman, E. Effron, Two-Phase Cocurrent Downflow in Packed Beds, Industrial & Engineering Chemistry Fundamentals 8 (1969) 63–71.

[82] P. Cognet, J. Berlan, G. Lacoste, P.-L. . Fabre, J.-M. . Jud, Application of metallic foams in an electrochemical pulsed flow reactor Part I: Mass transfer performance, Journal of Applied Electrochemistry 25 (1995) 1105–1112.

[83] D.E. Rivero, Physical properties of sugar solutions and hydrogenation reactions of sugar into sugar alcohols over Ru/C monolithic catalysts, M.Sc. thesis, Åbo Akademi University, Turku/Åbo, 2009.

[84] F. Lali, Characterization of foam catalysts as packing for tubular reactors, Chemical Engineering and Processing: Process Intensification 105 (2016) 1–9.

[85] T. Truong Huu, R. Philippe, P. Nguyen, D. Edouard, D. Schweich, Radial Dispersion in Liquid Upflow through Solid SiC Foams, Industrial & Engineering Chemistry Research 50 (2011) 4329–4334.

[86] P. D. Plessis, Pore scale modelling for flow through different types of porous environment, in Heat and Mass Transfer in Porous Media, Elsevier Amsterdam 249-262 (1992).

[87] C.R. Wilke, P. Chang, Correlation of diffusion coefficients in dilute solutions, AIChE Journal 1 (1955) 264–270.

[88] G. Ambrosio, N. Bianco, W.K.S. Chiu, M. Iasiello, V. Naso, M. Oliviero, The effect of open-cell metal foams strut shape on convection heat transfer and pressure drop, Applied Thermal Engineering 103 (2016) 333–343.

ISBN 978-952-12-4049-2 (printed version)
ISBN 978-952-12-4050-8 (electronic version)
ISSN 2669-8315 2670-0638
Acta technologiae chemicae Aboensia 2021 A/2